Quantum phase transition of the SU(4) Heisenberg model on a triangular lattice

Shay Nadel

Quantum phase transition of the SU(4) Heisenberg model on a triangular lattice

Research Thesis

Submitted in partial fulfillment of the requirements
for the degree of Master of Science in Physics

Shay Nadel

Submitted to the Senate
of the Technion — Israel Institute of Technology
Haifa
September 2025
Tishri 5785

This research was carried out under the supervision of Prof. Anna Keselman and Prof. Daniel Podolsky, in the Faculty of Physics.

The author of this thesis states that the research, including the collection, processing and presentation of data, addressing and comparing to previous research, etc., was done entirely in an honest way, as expected from scientific research that is conducted according to the ethical standards of the academic world. Also, reporting the research and its results in this thesis was done in an honest and complete manner, according to the same standards.

The Technion's funding of this research is hereby acknowledged.

Contents

List of Figures

Abstract

Frustrated magnetic systems, where the lattice geometry prevents the simultaneous satisfaction of all local interactions, are of increasing interest in condensed matter physics for their ability to host exotic quantum phases. This tendency toward quantum behavior can be amplified in systems with $SU(N)$ local symmetry with $N > 2$, as the enlarged symmetry boosts quantum fluctuations that can destabilize simple mean-field descriptions.

As a concrete realization of these principles we study the $SU(4)$ antiferromagnetic Heisenberg model on a triangular lattice with nearest-neighbor (NN) and next-nearest-neighbor (NNN) interactions. This system exhibits a competition between two distinct ground state phases depending on the interaction strengths.

For strong NNN interactions, the system is stabilized in the natural extension of classical antiferromagnetic order to $SU(4)$ systems. This phase is called the $SU(4)$ Néel phase, where the mean-field order consists of a four-sublattice arrangement with each sublattice occupied by a different $SU(4)$ flavor. As NNN interactions weakens, quantum fluctuations break this classical ordered phase. For NN interactions only, recent Variational Monte Carlo studies reveal that the ground state is fundamentally different: an exotic phase with an unconventional mean-field structure. This structure breaks both translational and $SU(4)$ flavor symmetries, forming a four-site parallelogram unit cell. This unit cell is composed of a single site in the $SU(4)$ fundamental representation and an entangled three-site triangle in the $SU(4)$ anti-fundamental representation. We refer to this phase as the Trimerized phase.

To provide an analytical description of this novel Trimerized phase, we employ a Multi-Boson Linear Flavor-Wave Theory (MBLFWT). This is the Holstein-Primakoff method for large S expansion, with Multi-Bosons serving as the baseline Bosonic description of the system. Remarkably, we find that this approach remains self-consistent across the entire range, from purely NN coupling to equal NN and NNN coupling strengths. This self-consistency validates our analytical framework for this quantum phase. Furthermore, it enables a systematic energy comparison between the competing Trimerized and Néel phases. We then compare the vacuum state energies, calculated using MBLFWT for the Trimerized phase and standard Schwinger-Bosons Linear Flavor-Wave Theory (LFWT) for the Néel phase. Through this comparison, we identify a critical coupling ratio where the energetically preferable phase switches from

Trimerized to Néel. Since both MBLFWT and LFWT remain self-consistent near this transition point, the energy crossing indicates a first-order quantum phase transition, revealing the complete phase diagram of this system.

Our work establishes Multi-Boson Flavor-Wave Theory as a theoretical framework for understanding entangled mean-field magnetic ordered phases, and provides crucial analytical insights into the competition between classical and quantum orders in frustrated magnets.

Chapter 1

Introduction

1.1 Motivation

The study of frustrated magnetic systems has captivated condensed matter physicists for decades, offering a window into exotic phases of matter that disobey classical ordering principles. Magnetic frustration arises when competing interactions prevent the system from simultaneously satisfying all local bonds, leading to macroscopic degeneracies and enhanced quantum fluctuations that can encourage novel quantum phases.

A paradigmatic example of geometric frustration is the antiferromagnetic Heisenberg model on the two-dimensional triangular lattice. In the classical $SU(2)$ case, the antiferromagnetic interactions between nearest neighbors cannot be simultaneously satisfied on every triangle of the lattice; while two spins can align antiferromagnetically, the third spin in each triangle remains frustrated, unable to point antiparallel to both neighbors.

Low dimensional systems with local interactions contain fewer bonds, which destabilize classical order. This has been established by the Mermin-Wagner theorem [5], stating that continuous symmetries cannot be spontaneously broken in one and two dimensions at finite temperature for short-range interactions. This theorem suggests that low-dimensional systems are inherently more susceptible to fluctuations, making them natural candidates for hosting quantum disordered phases such as spin liquids or other exotic quantum states that lack classical long-range order.

The interplay between frustration and dimensionality is further enriched when we extend beyond the familiar $SU(2)$ spin systems to higher symmetry groups.
$SU(N)$ spin models with $N > 2$ have emerged as particularly fertile ground for discovering new quantum phases, as the larger local Hilbert space enhances quantum fluctuations.

$SU(N)$ systems are not merely theoretical constructs; they appear in various physical contexts. In cold atomic systems, the $SU(N)$ symmetry can arise from nuclear degeneracy, where N represents the number of hyperfine states accessible to the atoms [1]. In transition metal compounds, orbital degrees of freedom can give rise to effective

$SU(N)$ models when combined with spin degrees of freedom [4, 7, 9]. These realizations make $SU(N)$ models relevant to experimental investigations.

The combination of geometric frustration, low dimensionality, and large N creates a good platform for enhanced quantum fluctuations. These systems can completely destroy classical order, leading instead to exotic quantum phases such as spin liquids, valence bond solids, and novel symmetry-broken phases that have no classical analogs.

In this context, the $SU(4)$ antiferromagnetic Heisenberg model on the two-dimensional triangular lattice represents an ideal testing ground for these ideas with nearest-neighbors and next-nearest-neighbors interactions. The system combines geometric frustration from the triangular geometry with the enhanced fluctuations inherent to $SU(4)$ symmetry.

Indeed, previous numerical studies have identified the Trimerized phase as a ground state of the system [8]. This phase competes with a classically mean-field ordered Néel phase [6].

Analytical description of the Trimerized phase may give new insights on entangled mean-field ordered phases, and reveal the full phase diagram of this system.

1.2 Research Question

We study the antiferromagnetic Heisenberg model of $SU(4)$ spins on the triangular lattice with a fundamental representation on each site. Previous results for nearest-neighbors (NN) interactions, obtained using variational Monte Carlo (VMC), show simultaneous trimerization and $SU(4)$ symmetry breaking in the ground state [8]. For large enough next-nearest-neighbors (NNN) interactions, exact diagonalization (ED) and linear flavor-wave theory suggest that an $SU(4)$ Néel ordered ground state emerges [6]. In this work, we use Multi-Bosons Flavor-Wave Theory (MBFWT) to investigate the transition between these two phases.

1.3 The Model

We consider the 2-dimensional triangular lattice with $SU(4)$ fundamental representation on each lattice site. The Hamiltonian of the model is

$$H = J_1 \sum_{\langle i,j \rangle} \sum_{\mu,\nu=1}^{4} T_i^{\mu\nu} T_j^{\nu\mu} + J_2 \sum_{\langle\langle i,j \rangle\rangle} \sum_{\mu,\nu=1}^{4} T_i^{\mu\nu} T_j^{\nu\mu}, \tag{1.1}$$

where $J_1, J_2 \geq 0$ are the superexchange coupling parameters of the nearest-neighbors and next-nearest-neighbors bonds respectively, and $(T_i^{\mu\nu})$ are the $SU(4)$ ladder operators on the local Hilbert space of lattice site i as defined in Sec. 2.1.1.

1.4 Previous Results

Previous studies of this model conjecture a few candidates for the ground state of the system, depending on the strength of next-nearest-neighbor interaction strength.

For large enough

$$J_2$$

, Penc et al. [6] conjecture the $SU(4)$ Néel (Sec. 1.5.2) as the ground state of the system. The results are obtained by Linear Flavor Wave expansion that is self-consistent for $J_2/J_1 > 0.12$. This is numerically supported by looking at the Tower of States (also known as the Anderson Tower) of a 12-site cluster using Exact Diagonalization. For $J_2/J_1 = 0.1$ the Tower of States holds, implying long-range order in the system. For $J_2 = 0$ the Tower of States breaks down, implying the absence of long-range order in the system. This paper conjectures spin liquid or valence bond solid with 12 site diamond unit cell as the competing ground state for small enough J_2.

More recent numerical work [2] for the case $J_2 = 0$ using Density Matrix Renormalization Group (DMRG) with Gutzwiller projected mean-field ansatz conjectures a stripy ground state.

However, new numerical results [8] using Variational Monte Carlo algorithm conjecture the Trimerized phase (Sec. 1.5.3) as the ground state of the system when $J_2 = 0$.

1.5 Competing Phases

In this work, we focus on the Néel and Trimerized suggested phases and investigate the competition between these two in an attempt to build the full phase diagram of this system.

1.5.1 Local Hilbert Space Visualization

We use colors to visualize a state in the system. Starting from the local Hilbert space, we assign colors representing the basis states of the local Hilbert space as depicted in Fig. 1.1. With a single particle in the fundamental $SU(4)$ representation, the local Hilbert space is 4 dimensional. Therefore, we use four different colors.

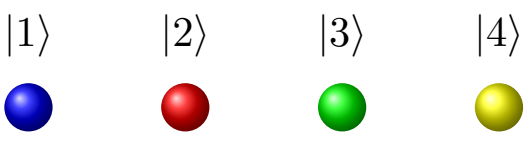

Figure 1.1: Visualization of the four basis state spanning the local Hilbert space by colors, matching $|1\rangle$ to blue, $|2\rangle$ to red, $|3\rangle$ to green and $|4\rangle$ to yellow.

To then visualize a classical state of the full system, we assign such colors to each of the lattice sites.

1.5.2 Néel Phase

This phase is a generalization of the well-known 2-sublattice formation of the $SU(2)$ antiferromagnetic Néel ordered phase, with up-spins on one sublattice and down-spins on the other.

A state in the quantum $SU(4)$ Néel phase [6] can be described as an ordered state with quantum fluctuations. This ordered state is called the mean-field Néel state.

The mean-field Néel state is composed of a four-sublattice structure, with each of the sublattices occupied by a different flavor. The unit cell of the original triangular lattice is extended to a 4-site parallelogram. This state breaks both the translation and $SU(4)$ symmetries; the original triangular lattice vectors are doubled in length, and the $SU(4)$ symmetry breaks to $U(1) \times U(1) \times U(1)$. A visualization of such a state is depicted in Fig. 1.2.

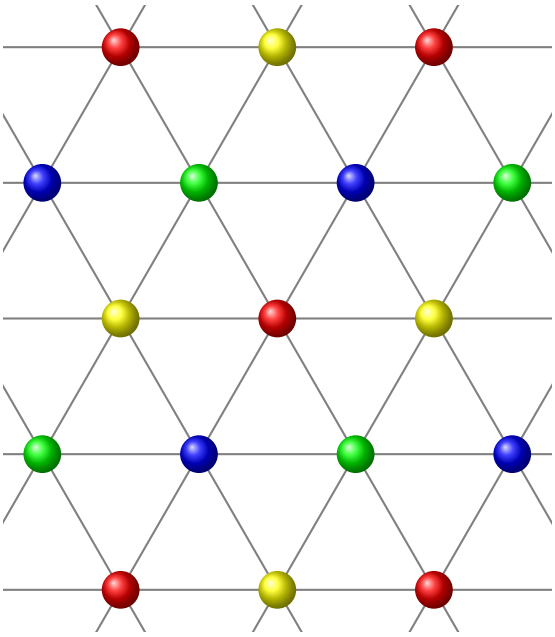

Figure 1.2: Mean-field $SU(4)$ Néel order visualization. A repetitive pattern of blue, red, green and yellow on a 4-site parallelograms using the notations in Fig. 1.1

This mean-field ordered state will be used in the explicit symmetry breaking of the Linear Flavor-Wave Theory of the Néel phase (Chapter 4).

1.5.3 Trimerized Phase

A state in the Trimerized phase [8] can be described as an ordered state with quantum fluctuations. This ordered state is called the Trimerized mean-field state.

Similar to the Néel state, the Trimerized mean-field state is ordered with a four-site parallelogram unit cell. The main difference is the inner structure within the unit cell. As opposed to a four-sublattice structure, the unit cell of the Trimerized state is composed of a single site in a specific flavor, and a three-site triangle in the fully

anti-symmetric superposition of the residual flavors.
For instance, choosing the local state $|4\rangle$ on the first sublattice, the second sublattice will be in the fully anti-symmetric superposition of states $|1\rangle, |2\rangle$ and $|3\rangle$. The state $|4\rangle$ is in the fundamental representation of $SU(4)$. The fully anti-symmetric superposition is in the anti-fundamental representation of $SU(4)$ and is denoted by $|\bar{4}\rangle$ indicating the missing flavor in the superposition. This choice is depicted in Fig. 1.3.

In this state, the $SU(4)$ symmetry breaks to $SU(3) \times U(1)$, creating an underlying quantum order with no classical analog.

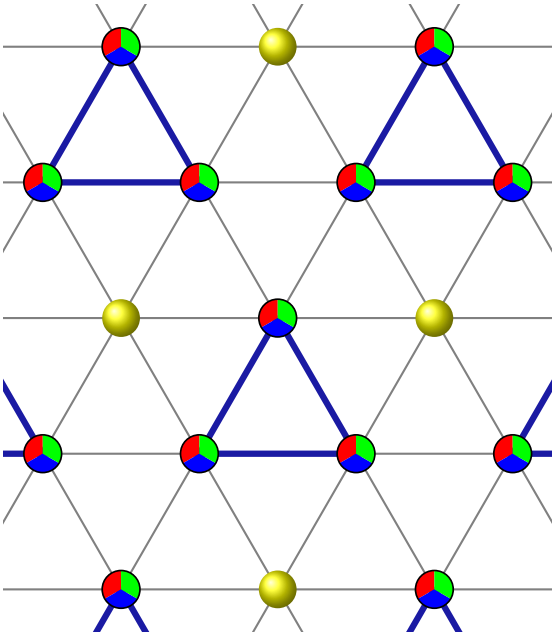

Figure 1.3: Visualization of the mean-field Trimerized phase with four-site parallelogram unit cell. The yellow circles depicts state $|4\rangle$, and the triangular three-sites formations with blue lines connecting them depicts state $|\bar{4}\rangle$. The circles on the triangle depicts the flavor content in the anti-symmetric superposition.

This mean-field ordered state will be used in the explicit symmetry breaking of the Multi-Bosons Linear Flavor-Wave Theory of the Trimerized phase (Chapter 3).

Chapter 2

Background

2.1 The SU(N) Group

The $SU(N)$ groups are widely investigated in physics. The $SU(2)$ and $SU(3)$ groups appear in the standard model, and are often used in particle physics.

In condensed matter physics, effective Hamiltonians are of main interest, often involving a local symmetry on a lattice described by $SU(N)$ group. $SU(2)$ local symmetry often emerges from the spin properties of the particles in the model, $SU(4)$ emerges from both spin and orbital (or valley) degrees of freedom [7, 9]. $SU(6)$ and $SU(10)$ emerges in systems of cold atoms corresponding to the degeneracy within the nuclei [1].

In this work, we focus on a local $SU(4)$ symmetry.

2.1.1 The SU(N) Generators and Representations

The $SU(N)$ group (Special Unitary $N \times N$ matrices) is generated by $N^2 - 1$ elements that are called the generators of the group.
The group can be generated by N^2 ladder operators of the group ($T^{\mu\nu}$), $\mu, \nu \in [N]$. They obey the commutation relations:

$$\left[T^{\mu\nu}, T^{\mu'\nu'}\right] = T^{\mu\nu'}\delta_{\mu'\nu} - T^{\mu'\nu}\delta_{\mu\nu'}. \tag{2.1}$$

for $\mu, \nu, \mu', \nu' \in [N]$.
A representation of a group (G) on a Hilbert space ($\mathcal{H}$), is a function $D : G \mapsto GL(\mathcal{H})$ that preserves the group action.

Any representation decomposes uniquely to a direct sum of irreducible representations (irrep.). For $SU(N)$, the fundamental representation of operators is the identity representation $D(g) = g$, matching a group element to an $N \times N$ special unitary matrix. The $SU(N)$ fundamental representation is an N dimensional vector. We label the fundamental representation states with N flavor indices, $|1\rangle, |2\rangle, \ldots, |N\rangle$.

2.1.2 The SU(2) Spin operators

The most familiar $SU(N)$ example in physics is $SU(2)$, which is widely used in spin systems.
The $SU(2)$ group is generated by 3 generators, S^x, S^y and S^z, obeying the angular momentum commutation relations

$$\left[S^\alpha, S^\beta\right] = i\epsilon^{\alpha\beta\gamma}S^\gamma \tag{2.2}$$

with $\alpha, \beta, \gamma \in [3]$ the spatial index, and $\epsilon^{\alpha\beta\gamma}$ the fully anti-symmetric Levi-Civita tensor. Einstein summation convention over repeating indices is applied. A different set of generators that are commonly used, are the $SU(2)$ ladder operators

$$S^\pm = S^x \pm iS^y \tag{2.3}$$

combined with S^z.
The fundamental representation of $SU(2)$ is the 2 dimensional spinor representation spanned by the eigenstates of S^z operator, $|\uparrow\rangle, |\downarrow\rangle$. These states can also be labeled with flavor indices $|1\rangle = |\uparrow\rangle, |2\rangle = |\downarrow\rangle$. The action of the spin operators in the fundamental representation is

$$S^z|\uparrow\rangle = \frac{1}{2}|\uparrow\rangle \quad , \quad S^z|\downarrow\rangle = -\frac{1}{2}|\downarrow\rangle \tag{2.4}$$

$$S^+|\uparrow\rangle = 0 \quad , \quad S^+|\downarrow\rangle = |\uparrow\rangle \tag{2.5}$$

$$S^-|\uparrow\rangle = |\downarrow\rangle \quad , \quad S^-|\downarrow\rangle = 0. \tag{2.6}$$

Matching the notation in Eq. (2.1), we relabel this set of operators as $S^{\mu\nu}$ with $\mu, \nu \in [2]$, where $S^{\mu\nu}$ annihilating flavor ν and creating flavor μ. This is summed up by

$$S^{\mu\nu}|\eta\rangle = \delta_{\nu\eta}|\mu\rangle \tag{2.7}$$

In this notation,

$$S^+ = S^{12} \tag{2.8}$$

$$S^- = S^{21} \tag{2.9}$$

$$S^z = \frac{1}{2}\left(S^{11} - S^{22}\right) \tag{2.10}$$

$$\tag{2.11}$$

and indeed these operators satisfy

$$\left[S^{\mu\nu}, S^{\mu'\nu'}\right] = S^{\mu\nu'}\delta_{\mu'\nu} - S^{\mu'\nu}\delta_{\mu\nu'}. \tag{2.12}$$

2.1.3 The SU(4) Spin Operators

In the fundamental representation of $SU(4)$, the local Hilbert space is 4 dimensional. States can be visualized by 4 different colors, as depicted in Fig. 1.1.

The $SU(4)$ ladder operators ($T^{\mu\nu}$) are defined on the local Hilbert space, and can be visualized with the colors scheme as in Fig. 2.1.

Figure 2.1: Visualization of the action of ladder operator $T^{\mu\nu}$ for the case $\mu = 2, \nu = 1$.

2.2 The SU(4) spin-orbital model

In this work, we focus on the Hamiltonian describing systems with coupled spin and orbital degrees of freedom:

$$\begin{aligned} H = &\sum_{\langle i,j \rangle} J_1 \left(2\vec{\sigma}_i \cdot \vec{\sigma}_j + \frac{1}{2}\right)\left(2\vec{\tau}_i \cdot \vec{\tau}_j + \frac{1}{2}\right) \\ &+ \sum_{\langle\langle i,j \rangle\rangle} J_2 \left(2\vec{\sigma}_i \cdot \vec{\sigma}_j + \frac{1}{2}\right)\left(2\vec{\tau}_i \cdot \vec{\tau}_j + \frac{1}{2}\right) \end{aligned} \tag{2.13}$$

This is a Kugel-Khomskii spin-orbital model [3] where $\vec{\sigma}_i$ and $\vec{\tau}_i$ are Pauli matrices corresponding to the the spin and orbital degrees of freedom, respectively, on lattice site i. The parameters $J_1, J_2 > 0$ represent the nearest-beighbor and next-nearest-neighbor superexchange coupling constants. When treated separately, these degrees of freedom exhibit an $SU(2) \times SU(2)$ symmetry.

The combined spin-orbital degrees of freedom constitute a 4 dimensional vector space at each lattice site.
We re-write this Hamiltonian in terms of the $SU(4)$ generators $T_i^{\mu\nu}$ acting on this space,

$$H = \sum_{i,j} J_{ij} \sum_{\mu,\nu=1}^{4} T_i^{\mu\nu} T_j^{\nu\mu} \tag{2.14}$$

This formulation explicitly demonstrates that the Hamiltonian possesses an enlarged $SU(4)$ symmetry.

2.3 Schwinger Bosons

The Schwinger Bosons of an $SU(N)$ group, are a set of hard-core bosonic field operators $(a_\mu, a_\mu^\dagger)$. These operators satisfy the canonical bosonic commutation relations (CCR)

$$\left[a_\mu, a_\nu^\dagger\right] = \delta_{\mu\nu} \tag{2.15}$$

and

$$\sum_{\mu=1}^{N} a_\mu^\dagger a_\mu = S, \tag{2.16}$$

with $S \in \mathbb{R}^+$ corresponding to the $SU(N)$ magnetic moment. For $SU(2)$ with a single particle per site $S = 1/2$. For our case of $SU(4)$ with a single particle per site in the fundamental representation, $S = 1$.
In the Schwinger Bosons approach, the ladder operators are defined by these bosonic field operators in the following way,

$$T^{\mu\nu} = a_\mu^\dagger a_\nu \tag{2.17}$$

matching both the action of the operators and satisfy Eq. (2.1).

2.3.1 The SU(2) Schwinger Bosons

The $SU(2)$ Schwinger bosons are a_1, a_2 and their satisfying $\left[a_\mu, a_\nu^\dagger\right] = \delta_{\mu\nu}$. $a_1^\dagger\,(a_2^\dagger)$ is the operator corresponding to creating a spin up (down) state

$$a_1^\dagger \left|0\right\rangle = \left|\uparrow\right\rangle \tag{2.18}$$
$$a_2^\dagger \left|0\right\rangle = \left|\downarrow\right\rangle \tag{2.19}$$
$$a_1 \left|0\right\rangle = a_2 \left|0\right\rangle = 0, \tag{2.20}$$

and satisfy a hard-core bosonic condition

$$\sum_{\mu=1}^{2} a_\mu^\dagger a_\mu = 2S. \tag{2.21}$$

with $S = 1/2$ for the fundamental representation.

2.3.2 The SU(4) Schwinger Bosons

The $SU(4)$ Schwinger Bosons in the fundamental representation, are $(a_\mu)_{\mu=1}^4$ hard-core bosonic operators satisfying

$$[a_\mu, a_\nu^\dagger] = \delta_{\mu\nu} \quad , \quad \sum_{\mu=1}^{4} a_\mu^\dagger a_\mu = 1. \tag{2.22}$$

2.4 Holstein-Primakoff Expansion

Using the Schwinger Bosons approach, Holstein-Primakoff method embeds the hard-core bosons operators in a spontaneously broken symmetric way. In the work we will

choose a specific flavor (4) about we write the hard-core bosons condition,

$$\sum_{\mu=1}^{4} a_\mu^\dagger a_\mu = S \tag{2.23}$$

Isolating flavor 4,

$$a_4^\dagger a_4 = S - \sum_{\mu\neq 4} a_\mu^\dagger a_\mu \tag{2.24}$$

and formally, we can expand in powers of $1/S$ having

$$a_4^\dagger, a_4 \approx \sqrt{S}\sqrt{1 - \frac{1}{S}\sum_{\mu\neq 4} a_\mu^\dagger a_\mu} \approx \sqrt{S} \tag{2.25}$$

Specifically in our case, $S = 1$ is the occupation number per site at quarter filling, this means that an expansion in $1/S = 1$ is not justified.
The justification comes posteriori with the requirement that the expectation value $\left\langle \sum_{\mu\neq 4} a_\mu^\dagger a_\mu \right\rangle$, which is the fluctuation around the vacuum state, is small. More than a method to solve, this may give a regime in which the expansion is valid.

2.5 Bogoliubov transformation

Given a system has a discrete translational symmetry, the crystal momentum quantum number $\boldsymbol{k}$ is well defined. The most general form of an Hermitian quadratic Hamiltonian in a set of field operators $\vec{\beta}_{\boldsymbol{k}} = \begin{pmatrix} \beta_{1,\boldsymbol{k}} & \beta_{2,\boldsymbol{k}} & \dots & \beta_{n,\boldsymbol{k}} \end{pmatrix}$ that satisfies this symmetry, can be written in a canonical form defined as

$$H = \mathcal{E}_N + \sum_{\boldsymbol{k}>0} \begin{pmatrix} \vec{\beta}_{\boldsymbol{k}}^\dagger & \vec{\beta}_{-\boldsymbol{k}} \end{pmatrix} \begin{pmatrix} \mathcal{N}_{\boldsymbol{k}} & \mathcal{A}_{\boldsymbol{k}} \\ \mathcal{A}_{\boldsymbol{k}}^\dagger & \mathcal{N}_{\boldsymbol{k}}^\dagger \end{pmatrix} \begin{pmatrix} \vec{\beta}_{\boldsymbol{k}} \\ \vec{\beta}_{-\boldsymbol{k}}^\dagger \end{pmatrix} \tag{2.26}$$

with $\mathcal{E}_N$ a constant term independent of the field operators, $\mathcal{N}_{\boldsymbol{k}}$ an $n \times n$ matrix associated with normal terms in the Hamiltonian ($\beta_i^\dagger \beta_j$ and $\beta_i \beta_j^\dagger$), $\mathcal{A}_{\boldsymbol{k}}$ an $n \times n$ matrix associated with anomalous terms in the Hamiltonian ($\beta_i \beta_j$ and $\beta_i^\dagger \beta_j^\dagger$).

For systems where the number of particles is conserved, there can be no anomalous terms. In these cases, transforming the system to this canonical form is redundant.

In the original model of this thesis, we enforce a single particle per lattice site, which implies the number of particles is conserved. Though, the Holstein-Primakoff approximation raises a field theory analysis, essentially treating the system in the Grand Canonical ensemble. The trade-off of this process yields a local chemical potential from the hard-core bosons condition.
As we use this expansion, there will exist anomalous terms, and so we are interested in diagonalizing these types of Hamiltonians.

The Bogoliubov transformation is essentially a symplectic transformation to diagonalize these types of Hamiltonians where the eigenvector field operators preserve the bosonic commutation relation.

Let

$$\boldsymbol{\gamma_k} = \begin{pmatrix} \vec{\beta}_{i,\boldsymbol{k}} \\ \vec{\beta}^{\dagger}_{i,-\boldsymbol{k}} \end{pmatrix} = \begin{pmatrix} \beta_{1,\boldsymbol{k}} & \dots & \beta_{n,\boldsymbol{k}} & \beta^{\dagger}_{1,-\boldsymbol{k}} & \dots & \beta^{\dagger}_{n,-\boldsymbol{k}} \end{pmatrix}^T \tag{2.27}$$

and $\beta_{i,\boldsymbol{k}}$ holding the bosonic canonical commutation relations (CCR), $\left[\beta_{i,\boldsymbol{k}}, \beta^{\dagger}_{j,\boldsymbol{k}'}\right] = \delta_{ij} \cdot \delta\left(\boldsymbol{k} - \boldsymbol{k}'\right)$.
Consider a general Hamiltonian in the canonical form as defined in Eq. (2.26). Let

$$H_{\boldsymbol{k}} = \begin{pmatrix} \mathcal{N}_{\boldsymbol{k}} & \mathcal{A}_{\boldsymbol{k}} \\ \mathcal{A}^{\dagger}_{\boldsymbol{k}} & \mathcal{N}_{-\boldsymbol{k}} \end{pmatrix} \tag{2.28}$$

and

$$\Gamma = \begin{pmatrix} \mathbb{1}_{n\times n} & \\ & -\mathbb{1}_{n\times n} \end{pmatrix} \tag{2.29}$$

This implies

$$\left[\gamma_{i,\boldsymbol{k}}, \gamma_{j,\boldsymbol{k}}\right] = 0 \quad , \quad \left[\gamma_{i,\boldsymbol{k}}, \gamma^{\dagger}_{j,\boldsymbol{k}}\right] = (\Gamma)_{ij} \tag{2.30}$$

Consider now a diagonalizing transformation $W_{\boldsymbol{k}}$ such that $W^{\dagger}_{\boldsymbol{k}} \hat{H}_{\boldsymbol{k}} W_{\boldsymbol{k}} = D_{\boldsymbol{k}} = \operatorname{diag}\left[\omega_{1,\boldsymbol{k}}, \omega_{2,\boldsymbol{k}}, \dots \omega_{2n,\boldsymbol{k}}\right]$ and creation/annihilation operators eigenvector $\boldsymbol{\xi_k} = \begin{pmatrix} \vec{\alpha}_{\boldsymbol{k}} \\ \vec{\alpha}^{\dagger}_{-\boldsymbol{k}} \end{pmatrix}$ with

$$\boldsymbol{\gamma_k} = W_{\boldsymbol{k}} \boldsymbol{\xi_k}. \tag{2.31}$$

Therefore,

$$\hat{H}_{\boldsymbol{k}} = \boldsymbol{\gamma}^{\dagger}_{\boldsymbol{k}} H_{\boldsymbol{k}} \boldsymbol{\gamma_k} = \boldsymbol{\xi}^{\dagger}_{\boldsymbol{k}} W^{\dagger}_{\boldsymbol{k}} H_{\boldsymbol{k}} W_{\boldsymbol{k}} \xi_{\boldsymbol{k}} = \boldsymbol{\xi}^{\dagger}_{\boldsymbol{k}} D_{\boldsymbol{k}} \boldsymbol{\xi_k} = \sum_{i=1}^{n} \omega_{i,\boldsymbol{k}} \alpha^{\dagger}_{i,\boldsymbol{k}} \alpha_{\boldsymbol{k}} + \omega_{i+n,-\boldsymbol{k}} \alpha_{i,-\boldsymbol{k}} \alpha^{\dagger}_{i,-\boldsymbol{k}} \tag{2.32}$$

To interpret this form as excitations, we must demand the correct CCR for $\alpha_{i,\boldsymbol{k}}$. This can be encapsulated in the condition

$$\left[\xi_{i,\boldsymbol{k}}, \xi_{j,\boldsymbol{k}}\right] = 0, \quad \left[\xi_{i,\boldsymbol{k}}, \xi^{\dagger}_{j,\boldsymbol{k}}\right] = (\Gamma)_{ij} \tag{2.33}$$

and so

$$\left[\xi_{i,\boldsymbol{k}}, \xi^{\dagger}_{j,\boldsymbol{k}}\right] = \sum_{m,n} (W_{\boldsymbol{k}})_{im} (W_{\boldsymbol{k}})^{*}_{jn} \left[\gamma_{m,\boldsymbol{k}}, \gamma^{\dagger}_{n,\boldsymbol{k}}\right] = \sum_{m,n} (W_{\boldsymbol{k}})_{im} (W_{\boldsymbol{k}})^{*}_{jn} (\Gamma)_{mn} \tag{2.34}$$

$$= \sum_{m,n} (W_{\boldsymbol{k}})_{im} (\Gamma)_{mn} \left(W^{\dagger}_{\boldsymbol{k}}\right)_{nj} = \left(W_{\boldsymbol{k}} \Gamma W^{\dagger}_{\boldsymbol{k}}\right)_{ij} = (\Gamma)_{ij} \tag{2.35}$$

which implies

$$W^{\dagger}_{\boldsymbol{k}} = \Gamma W^{-1}_{\boldsymbol{k}} \Gamma \tag{2.36}$$

Substituting in equation 2.32,

$$\hat{H}_{\boldsymbol{k}} = \boldsymbol{\xi}_{\boldsymbol{k}}^{\dagger}\Gamma W_{\boldsymbol{k}}^{-1}\Gamma H_{\boldsymbol{k}} W_{\boldsymbol{k}}\boldsymbol{\xi}_{\boldsymbol{k}} = \boldsymbol{\xi}_{\boldsymbol{k}}^{\dagger} D_{\boldsymbol{k}}\boldsymbol{\xi}_{\boldsymbol{k}} \tag{2.37}$$

and so,

$$\Gamma W_{\boldsymbol{k}}^{-1}\Gamma H_{\boldsymbol{k}} W_{\boldsymbol{k}} = D_{\boldsymbol{k}} \implies W_{\boldsymbol{k}}^{-1}\Gamma H_{\boldsymbol{k}} W_{\boldsymbol{k}} = \Gamma D_{\boldsymbol{k}} \tag{2.38}$$

Thus, to find the vacuum state and excitations, we diagonalize $\Gamma H_{\boldsymbol{k}}$ and then multiply from the left the resulting diagonal matrix $\Gamma D_{\boldsymbol{k}}$ by Γ again to retrieve $D_{\boldsymbol{k}}$.

2.5.1 Vacuum state energy

The ground state energy of the Hamiltonian in Eq. (2.26), which is the vacuum state of the $\alpha_{m,\boldsymbol{k}}$ operators, is the sum of $\mathcal{E}_N$ that comes from reshaping a given Hamiltonian to the canonical form in Eq. (2.26) and the normal ordering from the Bogoliubov transformation.

The former will be explicitly derived for our model. For the latter, we plug in Eq. (2.32) into Eq. (2.26), and get after using the canonical commutation relations of the $\alpha_{m,\boldsymbol{k}}$ operators,

$$\begin{aligned} H &= \mathcal{E}_N + \sum_{\boldsymbol{k}>0}\sum_{i=1}^{n}\left(\omega_{i,\boldsymbol{k}}\alpha_{i,\boldsymbol{k}}^{\dagger}\alpha_{i,\boldsymbol{k}} + \omega_{i,-\boldsymbol{k}}\alpha_{i,-\boldsymbol{k}}^{\dagger}\alpha_{i,-\boldsymbol{k}} + \omega_{i,-\boldsymbol{k}}\right) \\ &= \mathcal{E} + \sum_{\boldsymbol{k}}\sum_{i=1}^{n}\omega_{i,\boldsymbol{k}}\alpha_{i,\boldsymbol{k}}^{\dagger}\alpha_{i,\boldsymbol{k}} \end{aligned} \tag{2.39}$$

with

$$\mathcal{E} = \mathcal{E}_N + \frac{1}{2}\sum_{\boldsymbol{k}}\sum_{i=1}^{n}\omega_{i,\boldsymbol{k}} \tag{2.40}$$

the vacuum state energy.

2.6 Multi-Bosons

In this section, we will define the Multi-Boson operators of 3 fundamental $SU(4)$ particles, their different irreducible representations and use them to write the spin operators in the Hamiltonian.

The Multi-Boson spin operators of 3 fundamental representation $SU(4)$ particles are $c_{\alpha\beta\gamma}$ $(\alpha,\beta,\gamma = 1,\ldots,4)$, satisfying

$$\left[c_{\alpha\beta\gamma}, c_{\alpha'\beta'\gamma'}^{\dagger}\right] = \delta_{\alpha\alpha'}\delta_{\beta\beta'}\delta_{\gamma\gamma'} \tag{2.41}$$

$$\sum_{\alpha\beta\gamma} c_{\alpha\beta\gamma}^{\dagger} c_{\alpha\beta\gamma} = S, \tag{2.42}$$

with $S \in \mathbb{R}$ a hard core Bosonic constraint. For the single particle per site, $S = 1$.

A visualization of these operators acting on the vacuum is depicted in Fig. 2.2.

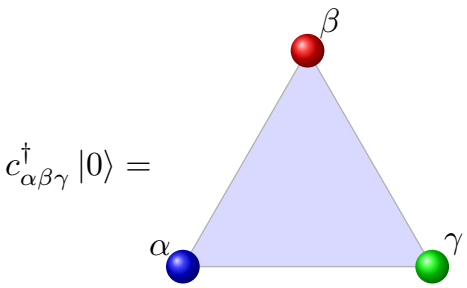

Figure 2.2: Multi-boson operators visualization. $c^\dagger_{\alpha\beta\gamma}$ creates state $|\alpha\rangle, |\beta\rangle$ and $|\gamma\rangle$ on the triangle in a specific ordering.

There are 64 $(= 4^3)$ unique $c_{\alpha\beta\gamma}$ operators representing the tensor product of 3 fundamental representation $SU(4)$ particles on a triangle.

2.6.1 Spin Operators

On a single triangle, we start from the $SU(4)$ fundamental representation Schwinger Bosons a_μ $(\mu = 1, \ldots, 4)$ to re-write the ladder operators:

$$T^{\mu\nu}_\ell = a^\dagger_{\mu,\ell} a_{\nu,\ell}. \tag{2.43}$$

with $\ell \in [3]$. These operators annihilate flavor ν of the fundamental representation and create flavor μ on site ℓ of the triangle.
A different way to write the same spin operators using the Multi-Boson operators,

$$T^{\mu\nu}_1 = \sum_{a,b=1}^{4} c^\dagger_{\mu ab} c_{\nu ab}, \quad T^{\mu\nu}_2 = \sum_{a,b=1}^{4} c^\dagger_{a\mu b} c_{a\nu b}, \quad T^{\mu\nu}_3 = \sum_{a,b=1}^{4} c^\dagger_{ab\mu} c_{ab\nu}. \tag{2.44}$$

As each of these operators is quadratic in the Multi-Boson operators, they can be re-written using representative matrices $S^{\mu\nu}_\ell$ with $\ell = 1, 2, 3$ in this specific basis. The spin operators become

$$T^{\mu\nu}_\ell = \sum_{m.n=1}^{64} c^\dagger_m \left(S^{\mu\nu}_\ell\right)_{mn} c_n \tag{2.45}$$

with $\left(S^{\mu\nu}_\ell\right)_{mn}$ the m-th row and n-th column matrix element of $S^{\mu\nu}_\ell$, and m an index of a specific $\alpha\beta\gamma$ index.

2.6.2 Irreducible representations

As the Hamiltonian is $SU(4)$ symmetric, Schur's lemma motivates us to work in the basis of irreducible representations. The irreducible representations of the tensor product of 3 fundamental representation $SU(4)$ are described via Young tableaux as follows,

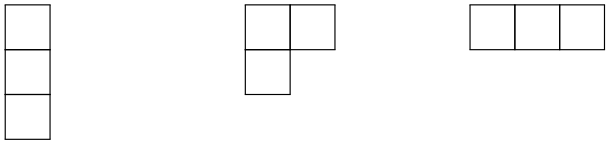

Anti-symmetric $(\bar{4})$ Mixed $2 \times (20_M)$ Symmetric (20_S)

To understand the Tableaux diagrams, each box describes an index. Boxes that are horizontally (vertically) aligned describe symmetric (anti-symmetric) interchanging between the respective indices of a state.
The dimensionality of the irreducible representation can be understood by combinatorial arguments with the rules as follows; each box is filled with a flavor index $\mu \in [4]$. Flavor indices must be non-decreasing moving right in the position of the boxes, and increasing moving down. In the $SU(4)$ irreducible representation notations we sum this with

$$(4) \otimes (4) \otimes (4) \sim (\bar{4}) \oplus 2 \cdot (20_M) \oplus (20_S) \tag{2.46}$$

with (4) the fundamental representation, $(\bar{4})$ the fully anti-symmetric representation, (20_M) the 3 particle mixed representation and (20_S) the 3 particle symmetric representation matching the Young Tablaux scheme. The fully anti-symmetric representation is also known as the anti-fundamental representation.

We define the Multi-Bosons operators in the irreducible representation basis, (b_m), with $m = 1, \ldots, 64$ an index of a state within the irrep. basis.

The connection between the two operators is via a unitary transformation U. This unitary transformation is constructed from Clebsh-Gordan coefficients and preserves the Bosonic canonical commutation relations, meaning

$$[b_m, b_n^\dagger] = \delta_{mn} \tag{2.47}$$

and the hard core bosonic constraint

$$\sum_{m=1}^{64} b_m^\dagger b_m = S. \tag{2.48}$$

Now we write the spin operators in terms of the b_m operators,

$$T_\ell^{\mu\nu} = \sum_{m,n=1}^{64} c_m^\dagger \left(S_\ell^{\mu\nu}\right)_{mn} c_n = \sum_{m,n=1}^{64} c_m^\dagger U^\dagger U \left(S_\ell^{\mu\nu}\right)_{mn} U^\dagger U c_n$$
$$= \sum_{m,n=1}^{64} b_m^\dagger \left(A_\ell^{\mu\nu}\right)_{m,n} b_n \tag{2.49}$$

with

$$A_\ell^{\mu\nu} = U S_\ell^{\mu\nu} U^\dagger. \tag{2.50}$$

2.7 Exclusion Rules for the Symmetry Broken Hamiltonian

In the Holstein-Primakoff expansion (Sec. 2.4), the symmetry of the system breaks explicitly. In our case, by choosing flavor 4 and its anti-fundamental respective state $\bar{4}$, the Hamiltonian breaks from $SU(4)$ symmetric to $SU(3)$ symmetric.
Therefore, the Hamiltonian needs to be $SU(3)$ invariant. This gives a restriction to the possible couplings of different bosonic operators.

The terms in the Hamiltonian need to be in the $SU(3)$ trivial representation. If a field operator β_m is in a specific irrep. of $SU(3)$, then $\beta_m^\dagger$ is in the conjugate representation.
This implies that $\beta_m \beta_n^\dagger$ terms are in the trivial representation if β_m and β_n are in the same irrep. Therefore, such terms are allowed.

On the contrast, to have anomalous terms such as $\beta_m \beta_m$ or $\beta_m^\dagger \beta_n^\dagger$, β_m and β_n needs to be in a conjugate representations.In terms of the matrices $\mathcal{A}_{\boldsymbol{k}}$ as defined in Eq. (2.26), this restricts the possible non-zero elements. This constraint breaks the Hilbert space $\mathcal{H}$ to a direct sum of spaces; with anomalous terms and without anomalous terms.

As the Bogoliubov transformation is redundant for Hamiltonians with no anomalous terms, we shall define the relevant subspace $\mathcal{D} \subset \mathcal{H}$ the subspace containing anomalous terms.

2.7.1 Irreducible Representations of SU(3)

As $SU(3)$ a subgroup of $SU(4)$, we map the irreducible representations of $SU(4)$ to irreducible representations of $SU(3)$,

$$(4) \sim (1) \oplus (3) \tag{2.51}$$
$$(\bar{4}) \sim (1) \oplus (\bar{3}) \tag{2.52}$$
$$(20_S) \sim (1) \oplus (3) \oplus (6) \oplus (10) \tag{2.53}$$
$$(20_M) \sim (3) \oplus (\bar{3}) \oplus (6) \oplus (8) \tag{2.54}$$

with (1) the trivial representation, (3) the fundamental representation, ($\bar{3}$) the anti-fundamental representation, and (6), (8) and (10) the respective dimensional representations of $SU(3)$.

To denote both the $SU(4)$ irrep. and $SU(3)$ irrep. of a field operator, we will use the notation $(SU(3))_{SU(4)}$. For example, the (3) representation coming from 20_S will be denoted as $(3)_{20_S}$.

2.7.2 Conjugate representations of SU(3)

From the relevant irreducible representations, (1) and (8) are self-conjugates and (3) is the conjugate to ($\bar{3}$). (6) and (10) do not have their conjugate representations in the relevant irreps.
Hence, possible anomalous terms can be non-zero only between field operators in the $(1)-(1), (3)-(\bar{3})$ and $(8)-(8)$ representations.

2.7.3 General Structure

The restrictions on the anomalous terms imply the relevant Hilbert space is composed of only states that are in the $(1)_{20_S}, (3)_4, (\bar{3})_{\bar{4}}, (3)_{20_S}, 2\cdot(3)_{20_M}, 2\cdot(\bar{3})_{20_M}$ and $2\cdot(8)_{20_M}$.

Chapter 3

Trimerized Phase

As the Trimer phase spontaneously breaks the symmetry, we follow the Holstein-Primakoff approach (Sec. 2.4). Using a Bosonic description of the system, we conduct a Bose condensation of the mean-field ordered state. Then, we apply a large S expansion, and get a flavor wave Hamiltonian.

To capture the entangled properties of the mean-field order, we shall use Schwinger Bosons and Multi Bosons as the baseline to create a Linear Flavor Wave theory. We will show that this yields a self-consistent theory all along the parameter space $J_2/J_1 \in [0, 1]$. This will support the claim of a first order phase transition that will be shown in Sec. 5 between the Trimer and Néel phases, revealing the full phase diagram of the system.

3.1 Explicit Broken Symmetry

The translational symmetry breaking of the Trimer phase creates a 4-site unit cell with an inner structure of a single site in the fundamental representation and 3-site triangle in the corresponding anti-fundamental representation as shown in Fig. 3.1.

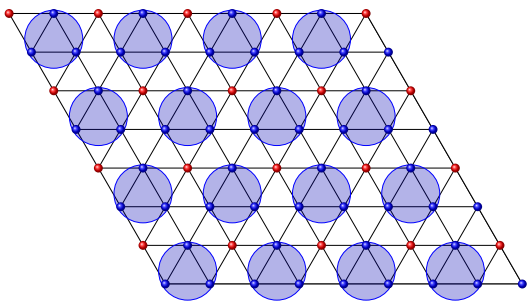

Figure 3.1: Trimer phase 4-site unit cell's inner structure of a single site and a triangle. Red dots corresponds to a single cite and three circled blue dots to the entangled triangle in the Trimer mean-field ordered state.

This inner structure creates a bipartite division of the triangular lattice, with sublattice A corresponding to the single site in the unit cell, and sublattice B to the three-site

triangle in the unit cell as depicted in Fig. 3.2.

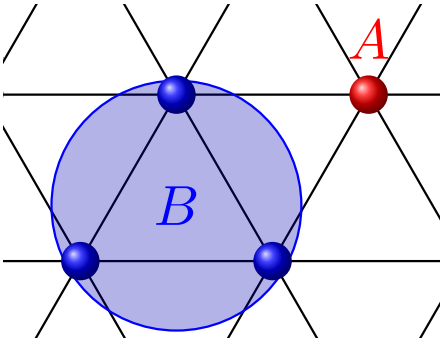

Figure 3.2: Bipartite structure of the Trimer phase. Sublattice A corresponds to the single site and sublattice B to the three-site triangle within the unit cell.

The original Hamiltonian

$$H = J_1 \sum_{\langle i,j \rangle} \sum_{\mu,\nu} T_i^{\mu\nu} T_j^{\nu\mu} + J_2 \sum_{\langle\langle i,j \rangle\rangle} \sum_{\mu,\nu} T_i^{\mu\nu} T_j^{\nu\mu}, \tag{3.1}$$

is written with i, j the triangular lattice indices.

In this extended unit cell structure, we change notations such that i is a unit cell index, and $\ell \in [4]$ is an additional spatial index of a specific site within the unit cell. The real space indices in this notation are uniquely defined via the set (i, ℓ).

We choose indices $1, 2$ and 3 to be a specific order of the triangle indices. As there is just one option for the single site, $\ell = 4$, it is uniquely defined by the unit cell index. To distinguish between sublattice A to sublattice B operators, we shall drop the extra index $\ell = 4$ when referring to the single site within the unit cell (sublattice A) as shown in Fig. 3.3

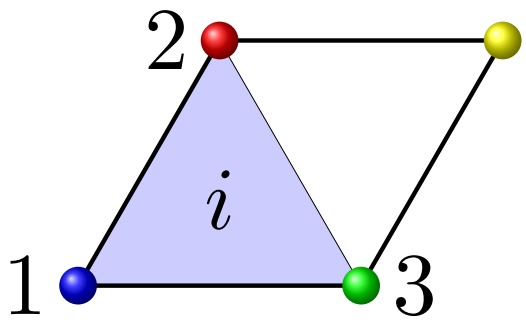

Figure 3.3: Enumeration of the Trimer phase's unit cell. $\ell \in [3]$ for the sites on the triangle, and the fourth site is uniquely defined within the unit cell.

Summarizing this change of notation:

$$i \mapsto \begin{cases} i & \text{Sublattice A} \\ (i,\ell) & \text{Sublattice B.} \end{cases} \tag{3.2}$$

The nearest neighbors and next nearest neighbors interactions couples sublattice A to sublattice B, and sublattice B to sublattice B only (Chapter A). Hence, the Hamiltonian can be written as:

$$H = H_{AB} + H_{BB} \tag{3.3}$$

$$H_{AB} = \sum_{\substack{i,j \\ \ell\in[3]}} \sum_{\mu\nu} J_{\vec{\chi}} T^{\mu\nu}_{(i,\ell)} T^{\nu\mu}_{j} \tag{3.4}$$

$$H_{BB} = \sum_{\substack{i,j \\ \ell_1,\ell_2\in[3]}} \sum_{\mu\nu} J_{\vec{\chi}} T^{\mu\nu}_{(i,\ell_1)} T^{\nu\mu}_{(j,\ell_2)}. \tag{3.5}$$

with i, j unit cell indices, ℓ, ℓ_1 and ℓ_2 indices on the triangle of the unit cell, $\vec{\chi}$ the real space vector connecting coupled sites in the interaction (Sec. A), and $J_{\vec{\chi}} \in \{0, J_1, J_2\}$ the respective coupling parameter.
Here onward, $T^{\mu\nu}_i$ corresponds to ladder operators on sublattice A, and $T^{\mu\nu}_{(i,\ell)}$ to ladder operators on sublattice B.

3.2 Bosonic Description

Rewriting the ladder operators with Bosonic description, we use Schwinger Bosons on sublattice A (Sec. 2.3.2), and Multi Bosons on sublattice B (Sec. 2.6.2).

The Schwinger Bosons on sublattice A are denoted as $(a_{\mu,i})_{\mu=1}^{4}$ and the Multi Bosons on sublattice B as $(b_{m,i})_{b=1}^{64}$ in the irreducible representation basis.

With a single particle per site,

$$\sum_{\mu=1}^{4} a^\dagger_{\mu,i} a_{\mu,i} = \sum_{m=1}^{64} b^\dagger_{m,i} b_{m,i} = S \tag{3.6}$$

gives us the hard-core Bosonic constraint with $S = 1$. The Ladder operators become

$$T^{\mu\nu}_i = a^\dagger_{\mu,i} a_{\nu,i} \tag{3.7}$$

$$T^{\mu\nu}_{(i,\ell)} = \sum_{m,n=1}^{64} \left(A^{\mu\nu}_\ell\right) b^\dagger_{m,i} b_{n,i} \tag{3.8}$$

with $A^{\mu\nu}_\ell$ as defined in Eq. (2.50).

Plugging these expressions in Eq. (3.4) and Eq. (3.5),

$$H_{AB} = \sum_{\substack{i,j \\ \ell\in[3]}} \sum_{\mu\nu} \sum_{m,n} J_{\vec{\chi}} \left(A_{\ell}^{\mu\nu}\right)_{mn} b_{m,i}^{\dagger} b_{n,i} a_{\nu,j}^{\dagger} a_{\mu,j} \tag{3.9}$$

$$H_{BB} = \sum_{\substack{i,j \\ \ell_1,\ell_2\in[3]}} \sum_{\mu\nu} \sum_{\substack{m,n \\ r,s}} J_{\vec{\chi}} \left(A_{\ell_1}^{\mu\nu}\right)_{mn} \left(A_{\ell_2}^{\nu\mu}\right)_{rs} b_{m,i}^{\dagger} b_{n,i} b_{r,j}^{\dagger} b_{s,j} \tag{3.10}$$

3.3 Multi-Bosons Linear Flavor-Wave Theory

As the mean-field ordered state of the trimer is a Bosonic condensate state of flavor 4 on sublattice A and flavor $\bar{4}$ on sublattice B, the Bosonic description in Sec. 3.2 gives a baseline to explicitly break the symmetry, which is the next step of the Holstein-Primakoff expansion.

By choosing these specific states and Eq. (3.6), we can isolate flavor 4 by doing so:

$$\sum_{\mu=1}^{4} a_{\mu,i}^{\dagger} a_{\mu,i} = S \implies a_{4,i}^{\dagger} a_{4,i} = S - \sum_{\mu\neq 4} a_{\mu,i}^{\dagger} a_{\mu,i} \tag{3.11}$$

Expanding in $1/S$ we approximate:

$$a_{4,i}^{\dagger}, a_{4,i} \approx \sqrt{S - \sum_{\mu\neq 4} a_{\mu,i}^{\dagger} a_{\mu,i}} \approx \sqrt{S}. \tag{3.12}$$

Creating a Bosonic condensation on sublattice A.

Doing the same on sublattice B, using again Eq. (3.6):

$$\sum_{m=1}^{64} b_{m,i}^{\dagger} b_{m,i} = S \implies b_{\bar{4},i}^{\dagger} b_{\bar{4},i} = S - \sum_{m\neq\bar{4}} b_{m,i}^{\dagger} b_{m,i} \tag{3.13}$$

and expanding in $1/S$:

$$b_{\bar{4},i}^{\dagger}, b_{\bar{4},i} \approx \sqrt{S - \sum_{m\neq\bar{4}} b_{m,i}^{\dagger} b_{m,i}} \approx \sqrt{S}. \tag{3.14}$$

giving the Bosonic condensate on sublattice B.

These two expansions are justified as long as the following conditions are satisfied:

$$\sum_{\mu\neq 4} \langle a_{\mu,i}^{\dagger} a_{\mu,i} \rangle < S \qquad \sum_{m\neq\bar{4}} \langle b_{m,i}^{\dagger} b_{m,i} \rangle < S \tag{3.15}$$

with $\langle \square \rangle$ the expectaiton value in the vacuum state. We then expand the Hamiltonian in powers of S,

$$H = H^{(2)} + H^{(1)} + \mathcal{O}(\sqrt{S}) \tag{3.16}$$

where $H^{(j)}$ is the term proportional to S^j in the expansion. Note $H^{3/2} = 0$ as the expansion is around an extremum of the energy, which has been calculated as well. (SN: think if to refer to appendix of this.)
Dropping $\mathcal{O}(\sqrt{S}$ terms, we get a Flavor-Wave Hamiltonian that is composed of terms quadratic in the field operators and a constant term that contributes to the vacuum state energy. The detailed derivation is in Chapter B.

3.3.1 General Structure

Using the notation in Eq. (B.10) and Eq. (B.9), we can write our Flavor-Wave Hamiltonian

$$H \approx \mathcal{E}_{\mathrm{N}} + \sum_{\boldsymbol{k}>0} \vec{\gamma}_{\boldsymbol{k}}^{\dagger} H_{\boldsymbol{k}} \vec{\gamma}_{\boldsymbol{k}}. \tag{3.17}$$

with $\{\boldsymbol{k} > 0\}$ a symbolic half of the First Brillouin Zone, $\vec{\gamma}_{\boldsymbol{k}} = \begin{pmatrix} \vec{b}_{\boldsymbol{k}} & \vec{a}_{\boldsymbol{k}} & \vec{b}_{-\boldsymbol{k}}^{\dagger} & \vec{a}_{-\boldsymbol{k}}^{\dagger} \end{pmatrix}^T$, and $\mathcal{E}_{\mathrm{N}}$ a term independent of the field operators.

If a projection of the Hilbert space is not coupled to the rest, and has no anomalous terms, then it is unitarily diagonalizable. As the vacuum state invariant under unitary transformations of the field operators, such subspaces can be treated separately.
Hamiltonians of this form are called normal Hamiltonians.
Hamiltonians with anomalous terms are called anomalous Hamiltonians.

As the Trimer phase has residual $SU(3)$ symmetry, each term in the Hamiltonian has to be in the trivial representation. This gives a restriction over the possible anomalous terms (Sec. 2.7).
Therefore, our Hamiltonian is a direct sum of a normal Hamiltonian and an anomalous Hamiltonian.

Focusing on the low energy physics, we project the Hamiltonian to the subspace that is connected via anomalous terms. This anomalous Hamiltonian is diagonalizable via a Bogoliubov transformation (Sec. 2.5). We shall denote this subspace $\mathcal{D}$.

In the following sections, we derive $H_{\boldsymbol{k}}$ and $\mathcal{E}_N$ on the relevant subspace only, by treating separately the AB and BB interactions.

$H_{\boldsymbol{k}}$, as defined in Eq. (3.17) is the coefficient matrix of the different terms in the Hamiltonian. In the basis of $\vec{\gamma}_{\boldsymbol{k}}$, the general structure of $H_{\boldsymbol{k}}$ breaks into blocks corresponding to either normal ($\mathcal{N}$) or anomalous ($\mathcal{A}$) terms in the Hamiltonian

$$H \approx \mathcal{E}_N + \sum_{\boldsymbol{k}>0} \vec{\gamma}_{\boldsymbol{k}}^{\dagger} \begin{pmatrix} \mathcal{N}_{\boldsymbol{k}} & \mathcal{A}_{\boldsymbol{k}} \\ \mathcal{A}_{\boldsymbol{k}}^{\dagger} & \mathcal{N}_{\boldsymbol{k}}^{\dagger} \end{pmatrix} \vec{\gamma}_{\boldsymbol{k}} \tag{3.18}$$

where $\mathcal{N}_{\boldsymbol{k}}$ and $\mathcal{A}_{\boldsymbol{k}}$ are Hermitian matrices over $\mathbb{C}$.

Note that $\mathcal{N}_{\boldsymbol{k}}, \mathcal{A}_{\boldsymbol{k}}$ are functions of J_1, J_2 and $(A_{\ell}^{\mu\nu})$, that are then diagonalized numerically using Bogoliubov transformation (Sec. 2.5).

From the structure of $\vec{\gamma}_{\boldsymbol{k}}$, both the normal and anomalous parts break into sub-blocks corresponding to terms connecting the different types of field operators, as depicted in Fig. 3.4.

$$\left(\begin{array}{cc:cc} \mathcal{N}_{\boldsymbol{k}}^{bb} & \mathcal{N}_{\boldsymbol{k}}^{ba} & \mathcal{A}_{\boldsymbol{k}}^{bb} & \mathcal{A}_{\boldsymbol{k}}^{ba} \\ \mathcal{N}_{\boldsymbol{k}}^{ab} & \mathcal{N}_{\boldsymbol{k}}^{aa} & \mathcal{A}_{\boldsymbol{k}}^{ab} & \mathcal{A}_{\boldsymbol{k}}^{aa} \\ \hline (\mathcal{A}_{\boldsymbol{k}}^{bb})^{\dagger} & (\mathcal{A}_{\boldsymbol{k}}^{ab})^{\dagger} & (\mathcal{N}_{\boldsymbol{k}}^{bb})^{*} & (\mathcal{N}_{\boldsymbol{k}}^{ba})^{*} \\ (\mathcal{A}_{\boldsymbol{k}}^{ba})^{\dagger} & (\mathcal{A}_{\boldsymbol{k}}^{aa})^{\dagger} & (\mathcal{N}_{\boldsymbol{k}}^{ab})^{*} & (\mathcal{N}_{\boldsymbol{k}}^{aa})^{*} \end{array}\right)$$

Figure 3.4: Structure of $H_{\boldsymbol{k}}$ in block form. The $\square^{bb}$ matrices are of dimension 63×63, the $\square^{aa}$ matrices are 3×3, the $\square^{ab}$ matrices are 63×3 and $\square^{ba}$ are 3×63.

(SN: Maybe add here the irrep content/ in the results)

3.3.2 Interactions

The separation in Eq. (3.9) and Eq. (3.10) shows three types of interactions: interactions between sublattice A and sublattice B (AB interactions), and interactions between sublattice B and sublattice B (BB interactions) that contain both inter-unit cell and intra-unit cell interactions.

Following Chapter B, both the AB interactions and the inter-unit cell BB interactions are derived from the Holstein-Primakoff method with the Schwinger-Bosons and Multi-Bosons as the Bosonic baseline, while the intra-unit cell BB interactions required a special treatment. As they consist of a separable Hamiltonian that is diagonal in the $SU(4)$ irreducible representation basis, we get the spectrum of a single unit cell, and only then conduct the Flavor-Wave approximation.

3.4 Bogoliubov Transformation

The Hamiltonian in Eq. (3.17) cannot be both diagonalized via a unitary transformation and to have it's eigenvector of Bosonic field operators satisfying the Bosonic canonical commutation relations. Thus, to get the vacuum state and dispersion of the Trimerized phase, we use the Bogoliubov transformation following Sec. 2.5.

Hence, to diagonalize $H_{\boldsymbol{k}}$ as defined in Eq. (3.17), let our diagonalizing transforma-

tion

$$\vec{\gamma}_{\boldsymbol{k}} = W_{\boldsymbol{k}} \vec{\xi}_{\boldsymbol{k}} \tag{3.19}$$

with $\vec{\xi}_{\boldsymbol{k}} = \begin{pmatrix} \vec{\alpha}_{\boldsymbol{k}} \\ \vec{\alpha}^{\dagger}_{-\boldsymbol{k}} \end{pmatrix}$ and $(\alpha_{m,\boldsymbol{k}})$ Bosonic field operators satisfying the Bosonic canonical commutation relations, with the Trimerized phase as their vacuum state. This transformation is symplectic. Meaning it satisfies:

$$W_{\boldsymbol{k}}^{-1} = \Gamma W_{\boldsymbol{k}}^{\dagger} \Gamma. \tag{3.20}$$

By plugging this in the Hamiltonian, we get

$$H = \mathcal{E} + \sum_{\boldsymbol{k}} \sum_{m \in \mathcal{D}} \omega_{m,\boldsymbol{k}} \alpha^{\dagger}_{m,\boldsymbol{k}} \alpha_{m,\boldsymbol{k}} \tag{3.21}$$

with $\mathcal{E}$ the Trimerized phase's vacuum state energy, $\omega_{m,\boldsymbol{k}}$ the dispersion, and $\alpha^{\dagger}_{m,\boldsymbol{k}} |0\rangle$ the excitations. All of these are derived in Chapter B, leading us to the results.

3.5 Results

As $H_{\boldsymbol{k}}\left(J_1, J_2, A_{\ell}^{\mu\nu}\right)$ a matrix over $\mathbb{C}$, we implement the analytical expression of this matrix numerically. The codes are accessible in https://github.com/shaynadel/MSc.-Thesis.

By diagonalizing the matrix, following Sec. 3.4, we get the spectrum and vacuum state properties as fluctuations, magnetization, and energy.

3.5.1 Spectrum

Plotting the lowest energy band on the First Brillouin Zone for $J_2 = 0$,

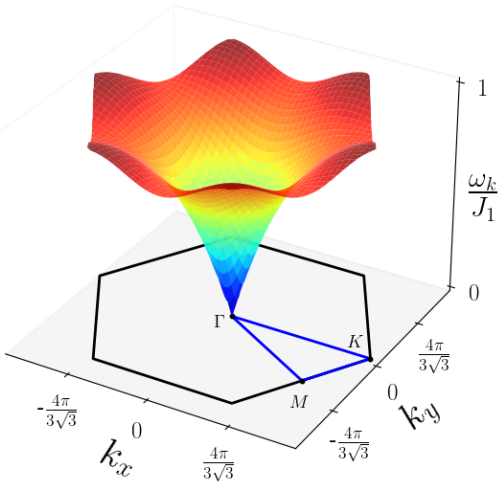

Figure 3.5: Trimer phase lowest energy band on the First Brillouin Zone for $J_2 = 0$. Colors emphasize the equal energy contours

(SN: Change to pdf and drop the HSP from the figure.) The energy at $(0, 0)$ of this excitation is 0, representing a Goldstone mode.
This band and higher excitations exhibit the point group symmetry of the triangular lattice. (SN: Figure what needs to be said here. Should I add plots of the higher excitations?)

As the Trimer phase breaks $SU(4) \mapsto SU(3) \times U(1)$, we expect 6 Goldstone modes when in the Trimer phase. This is because $SU(4)$ has $4^2 - 1 = 15$ generators, $SU(3)$ has $3^2 - 1 = 8$ and $U(1)$ has 1, and thus the number of Goldstone modes is $15 - (8 + 1) = 6$. Therefore, an interesting check for stability of the phase is to calculate the number of Goldstone modes as function of J_2.

A plot of the 6 lowest bands as function of J_2 is depicted in Fig. 3.6.

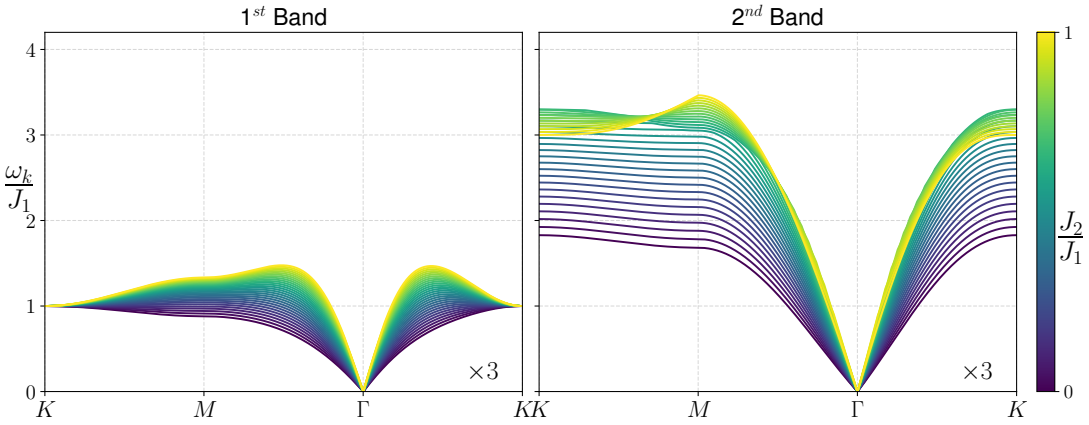

Figure 3.6: 6 Lowest energy bands on the High Symmetry Path as function of J_2/J_1. For each value of J_2, the lowest band is 3 times degenerate and so does the second lowest.

Each of the 6 lowest bands has zero energy at Γ, implying there are 6 Goldstone modes all along $J_2/J_1 \in [0, 1]$.

3.5.2 Fluctuations

The quantum fluctuations in the ground state are the expectation values of the occupation number of the residual flavors after conducting the Bose condensate. Meaning,

$$\langle a^\dagger a \rangle = \frac{1}{N} \sum_{\mathbf{k}} \sum_{\mu \neq 4} \langle a^\dagger_{\mu,\mathbf{k}} a_{\mu,\mathbf{k}} \rangle \tag{3.22}$$

$$\langle b^\dagger b \rangle = \frac{1}{N} \sum_{\mathbf{k}} \sum_{m \neq \bar{4}} \langle b^\dagger_{m,\mathbf{k}} b_{m,\mathbf{k}} \rangle \tag{3.23}$$

(SN: Should I elaborate on the calculation here or appendix?)

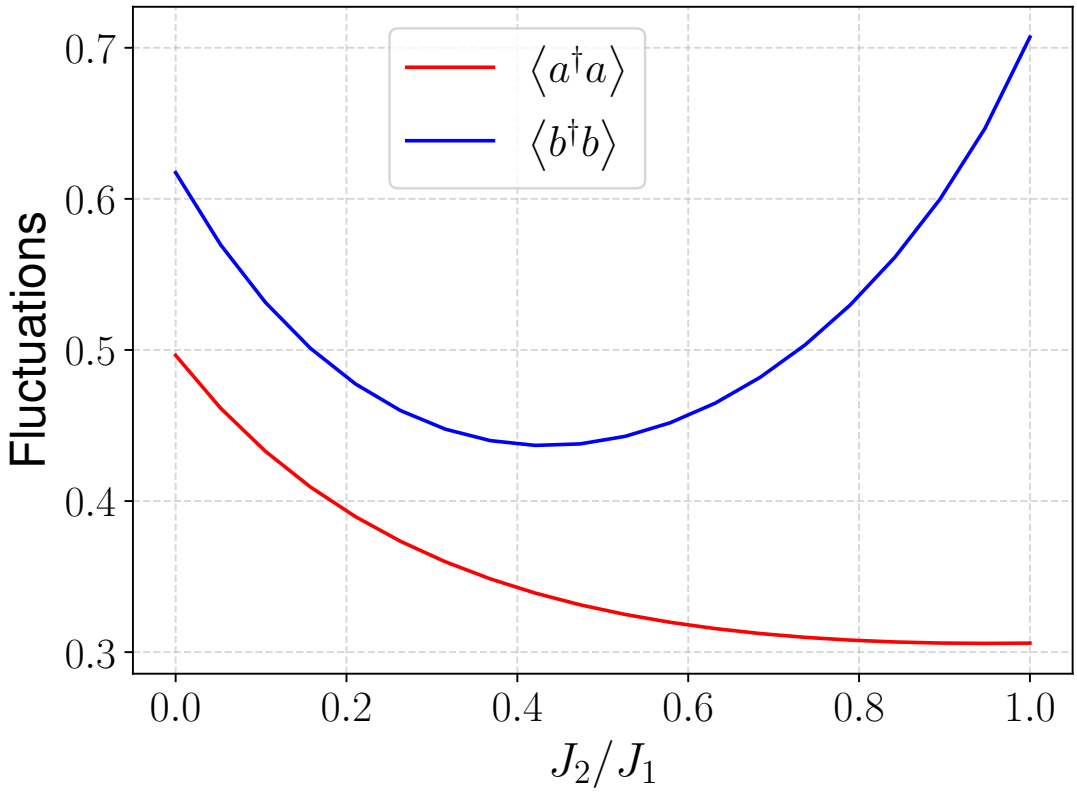

Figure 3.7: Trimer phase fluctuations on each of the sublattices as function of J_2/J_1.

This implies that for $J_2/J_1 \in [0, 1]$ both fluctuations are smaller than 1. Hence, the self-consistent conditions (Eq. (3.15)) hold all along the parameter space.

3.5.3 Magnetization

The $SU(4)$ magnetic moments on each of the sublattices are calculated as $3/4 - \langle a^\dagger a \rangle$ and $3/4 - \langle a^\dagger a \rangle$. The results as a function of J_2/J_1 are depicted in Fig. 3.8, exhibiting

a ferrimagnetic behavor all along the parameter space.

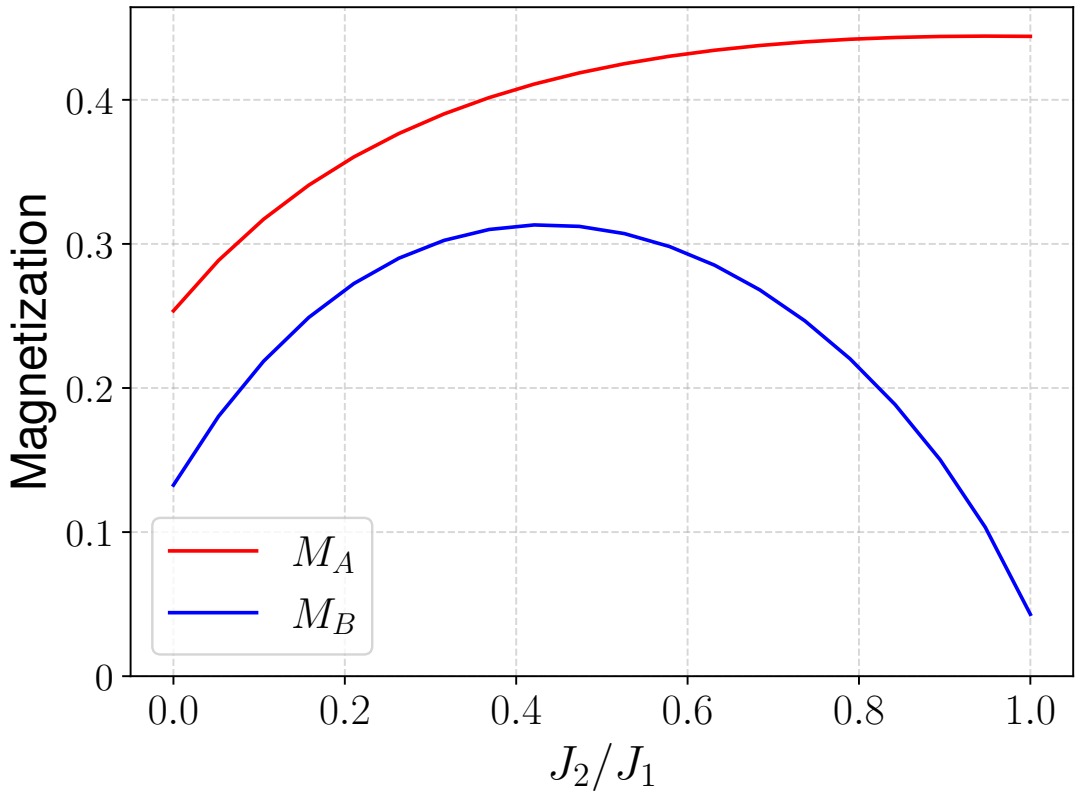

Figure 3.8: Trimer phase magnetic moment on each of the sublattices as function of J_2/J_1.

3.5.4 Vacuum State Energy

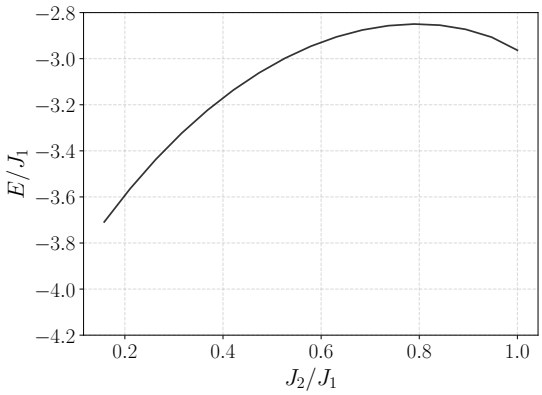

Figure 3.9: Vacuum state energy of the Trimer phase as function of J_2/J_1.

Chapter 4

Néel Phase

As the Néel phase spontaneously breaks the symmetry, we follow the Holstein-Primakoff approach (Sec. 2.4). Using a Bosonic description of the system, we conduct a Bose condensation of the mean-field ordered state. Then, we apply a large S expansion, and get a flavor wave Hamiltonian.

We shall use Schwinger Bosons as the baseline to create a Linear Flavor Wave Theory, and calculate the vacuum state energy of this phase. We will use these results in Sec. 5 to show a conjectured first order phase transition between the Trimer phase and the Néel phase.

4.1 Néel Explicit Broken Symmetry

The translational symmetry breaking of the Néel phase creates a 4-site unit cell as shown in Fig. 4.1.

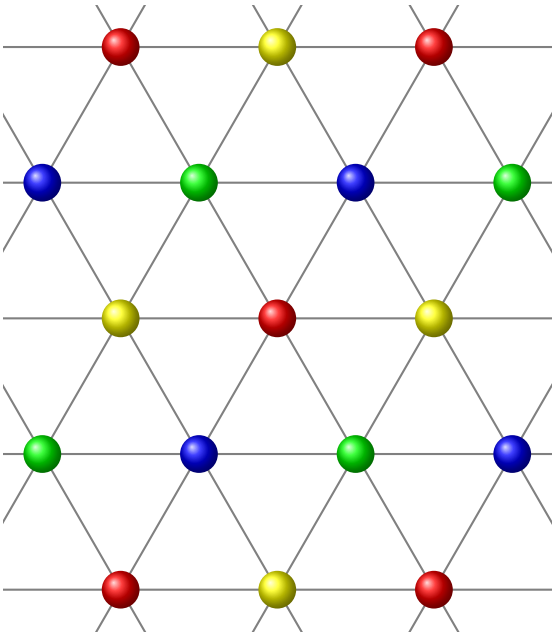

Figure 4.1: Néel phase mean-field order for a specific choice of colors representing different flavors.

The original Hamiltonian

$$H = J_1 \sum_{\langle i,j \rangle} \sum_{\mu,\nu} T_i^{\mu\nu} T_j^{\nu\mu} + J_2 \sum_{\langle\langle i,j \rangle\rangle} \sum_{\mu,\nu} T_i^{\mu\nu} T_j^{\nu\mu}, \tag{4.1}$$

is written with i, j the triangular lattice indices.

In this extended unit cell structure, we change notations such that i is a unit cell index, and $\ell \in [4]$ is an additional spatial index of a specific site within the unit cell. The real space indices in this notation are uniquely defined via the set (i, ℓ).

We choose indices $1, 2, 3$ and 4 to be a specific order of the parallelogram structure of the unit cell, as depicted in Fig. 4.2.

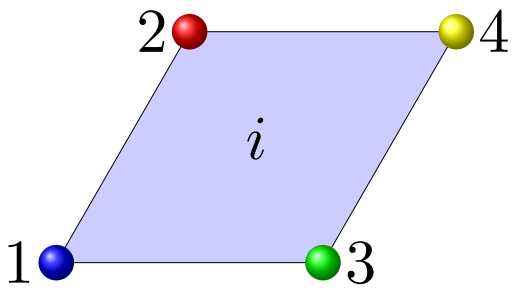

Figure 4.2: Enumeration of the Néel phase unit cell. Index i refers to an enumeration of the unit cell, and $\ell \in [4]$ for a specific site within the unit cell.

In this notation, the Hamiltonian can be written as:

$$H = \sum_{i,j} \sum_{\ell_1,\ell_2} \sum_{\mu,\nu} J_{\vec{\chi}} T^{\mu\nu}_{(\ell_1,i)} T^{\nu\mu}_{(\ell_2,j)} \tag{4.2}$$

with i, j unit cell indices, ℓ_1 and ℓ_2 indices of sites within the parallelogram of the unit cell, $\vec{\chi}$ the real space vector connecting coupled sites in the interaction, and $J_{\vec{\chi}} \in \{0, J_1, J_2\}$ the respective coupling parameter.

4.2 Bosonic Description

Using Schwinger Bosons in the fundamental representation of $SU(4)$ on each of the lattice site (Sec. 2.3.2), $(a_{\mu,\ell,i})$ with $\mu \in [4]$ flavor index, $\ell \in [4]$ spatial index within the unit cell and i unit cell index, we rewrite the ladder operators:

$$T^{\mu\nu}_{(i,\ell)} = a^\dagger_{\mu,\ell,i} a_{\nu,\ell,i}. \tag{4.3}$$

The Schwinger Bosons satisfy the hard-core Bosonic constraint,

$$\sum_{\mu=1}^{4} a^\dagger_{\mu,\ell,i} a_{\mu,\ell,i} = S \tag{4.4}$$

where, for the case of a single particle per site, $S = 1$.

Our Hamiltonian becomes:

$$\begin{aligned} H &= \sum_{i,j} \sum_{\ell_1,\ell_2} \sum_{\mu,\nu} J_{\vec{\chi}} T^{\mu\nu}_{(\ell_1,i)} T^{\nu\mu}_{(\ell_2,j)} \\ &= \sum_{i,j} \sum_{\ell_1,\ell_2} \sum_{\mu,\nu} J_{\vec{\chi}} a^\dagger_{\mu,\ell_1,i} a_{\nu,\ell_1,i} a^\dagger_{\nu,\ell_2,j} a_{\mu,\ell_2,j} \end{aligned} \tag{4.5}$$

with $\vec{\chi}$ the real space vector of the respective bond, and $J_{\vec{\chi}} \in \{0, J_1, J_2\}$ depending on the bond.

4.3 Linear Flavor Wave Theory

As the mean-field ordered state of the Néel phase is a Bosonic condensate state of 4-sublattice Néel pattern, such that each sublattice populates different flavor.
We shall choose flavor $\mu = \ell$ on site $\ell \in [4]$ within the unit cell to be the condensate. For instance, flavor 1 on site 1, 2 on two, and so on.

The Bosonic description in Sec. 4.2 gives a baseline to explicitly break the symmetry, which is the next step of the Holstein-Primakoff expansion.

By choosing these specific states and Eq. (4.4), we can isolate the respective flavor

by doing so:

$$a^{\dagger}_{\ell,\ell,i}a_{\ell,\ell,i} = S - \sum_{\mu\neq\ell} a^{\dagger}_{\mu,\ell,i}a_{\mu,\ell,i} \tag{4.6}$$

and by expanding in powers of $1/S$,

$$a^{\dagger}_{\ell,\ell,i}, a_{\ell,\ell,i} \approx \sqrt{S - \sum_{\mu\neq\ell} a^{\dagger}_{\mu,\ell,i}a_{\mu,\ell,i}} \approx \sqrt{S} \tag{4.7}$$

creating a Bosonic condensation on each of the sublattices.

These 4 expansions are justified as long as

$$\sum_{\mu\neq\ell}\langle a^{\dagger}_{\mu,\ell,i}a_{\mu,\ell,i}\rangle < S \tag{4.8}$$

with $\langle\square\rangle$ the expectation value in the vacuum state. We then expand the Hamiltonian in powers of S. Dropping lower orders than linear in S, we get a quadratic Hamiltonian in the field operators, that we call the Flavor Wave Hamiltonian,

$$H_{FW} = \mathcal{E}(J_1, J_2) + \sum_{\boldsymbol{k}}\sum_{\ell_1<\ell_2} \omega_{\ell_1,\ell_2}(\boldsymbol{k})\,\alpha^{\dagger}_{\ell_1,\ell_2,\boldsymbol{k}}\alpha_{\ell_1,\ell_2,\boldsymbol{k}} \tag{4.9}$$

with

$$\omega_{\ell_1,\ell_2}(\boldsymbol{k}) = 2S\sqrt{(J_1+J_2)^2 - \left(J_1\cos\left(\boldsymbol{k}\cdot\vec{\chi}^{nn}_{\ell_1\ell_2}\right) + J_2\cos\left(\boldsymbol{k}\cdot\vec{\chi}^{nnn}_{\ell_1\ell_2}\right)\right)^2}, \tag{4.10}$$

$(\alpha_{\ell_1,\ell_2,\boldsymbol{k}})$ Bosonic field operators satisfying

$$\left[\alpha_{\ell_1,\ell_2,\boldsymbol{k}}, \alpha^{\dagger}_{\ell_1',\ell_2',\boldsymbol{k}'}\right] = \delta_{\ell_1,\ell_1'}\delta_{\ell_2,\ell_2'}\delta(\boldsymbol{k}-\boldsymbol{k}') \tag{4.11}$$

and

$$\mathcal{E} = S\sum_{\boldsymbol{k}}\sum_{\ell_1<\ell_2}\left[2\sqrt{(J_1+J_2)^2 - J_1\left(\cos\left(\boldsymbol{k}\cdot\vec{\chi}^{nn}_{\ell_1,\ell_2}\right) + J_2\cos\left(\boldsymbol{k}\cdot\vec{\chi}^{nnn}_{\ell_1,\ell_2}\right)\right)^2} - 2(J_1+J_2)\right] \tag{4.12}$$

with $\vec{\chi}^{nn}_{\ell_1,\ell_2}$ vector connecting sites ℓ_1 to ℓ_2 as nearest neighbors and $\vec{\chi}^{nnn}_{\ell_1,\ell_2}$ next nearest neighbors.

4.4 Results

4.4.1 Self Consistency

Following [6], the self consistent condition in Eq. (4.8) is satisfied as $J_2/J_1 > 0.12$.

4.4.2 Vacuum State Energy

Calculating the vacuum state energy of the Néel phase as function of J_2:

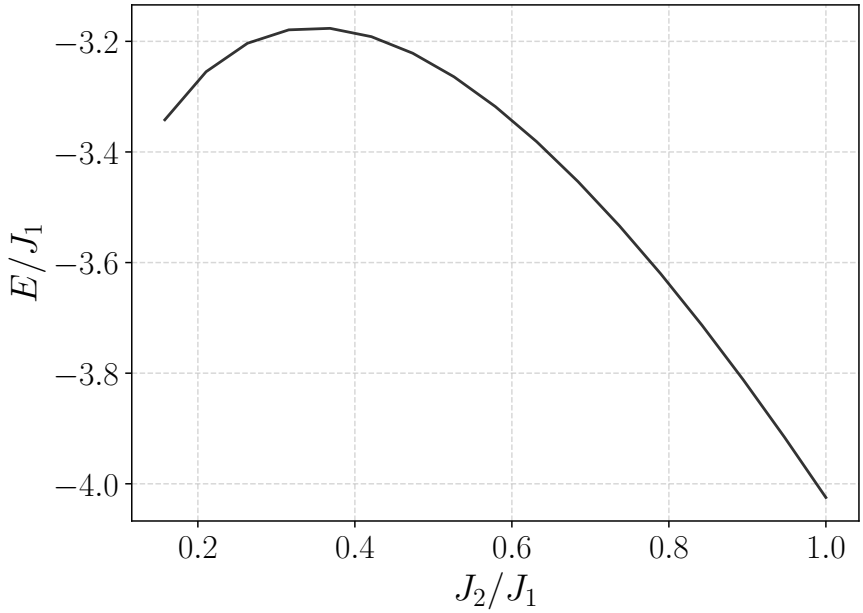

Figure 4.3: Néel state vacuum energy as function of J_2/J_1.

Chapter 5

Discussion

5.1 Phase transition

Concluding the results from Sec. 3.5.2 and [6], in the segment $J_2/J_1 \in [0.12, 1]$, both Flavor Wave Theories are self-consistent.

The comparison of the vacuum state energy of the Trimer phase (Sec. 3.5.4) and the Néel phase (Sec. 4.4.2) on this segment is depicted in figure Fig. 5.1.

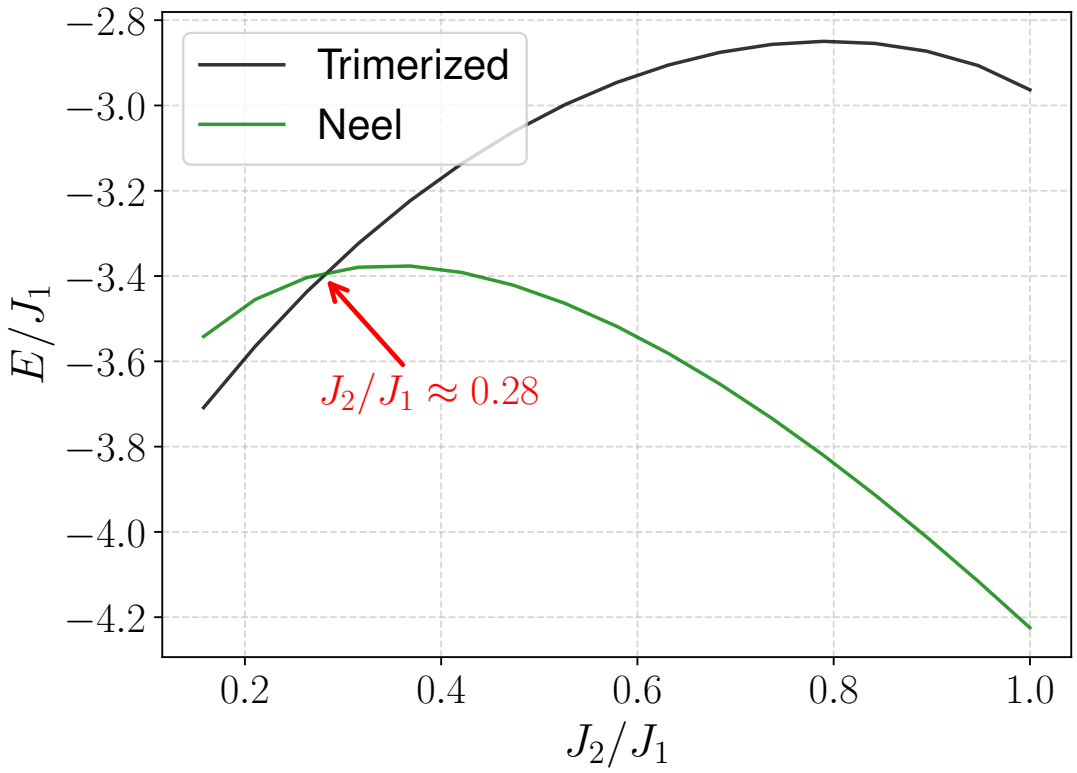

Figure 5.1: Vacuum state energy of the Néel and Trimerized phase as function of J_2/J_1.

The intersection of the two phases occurs at roughly 0.28, where below this value the Trimerized phase is energetically preferable, and when above, the Néel phase is.

This conjectures a first order phase transition between the two phases.

5.2 Band Crossing

In the spectrum of the 6 lowest bands of the Trimer expansion, as depicted in Fig. 3.6, the energies monotonically increase as function of J_2/J_1 until roughly $J_2/J_1 \approx 0.75$. Checking the full band structure at a specific non-degenerate point, we plot the full spectrum of the Trimer phase as function of J_2/J_1 as shown in Fig. 5.2.

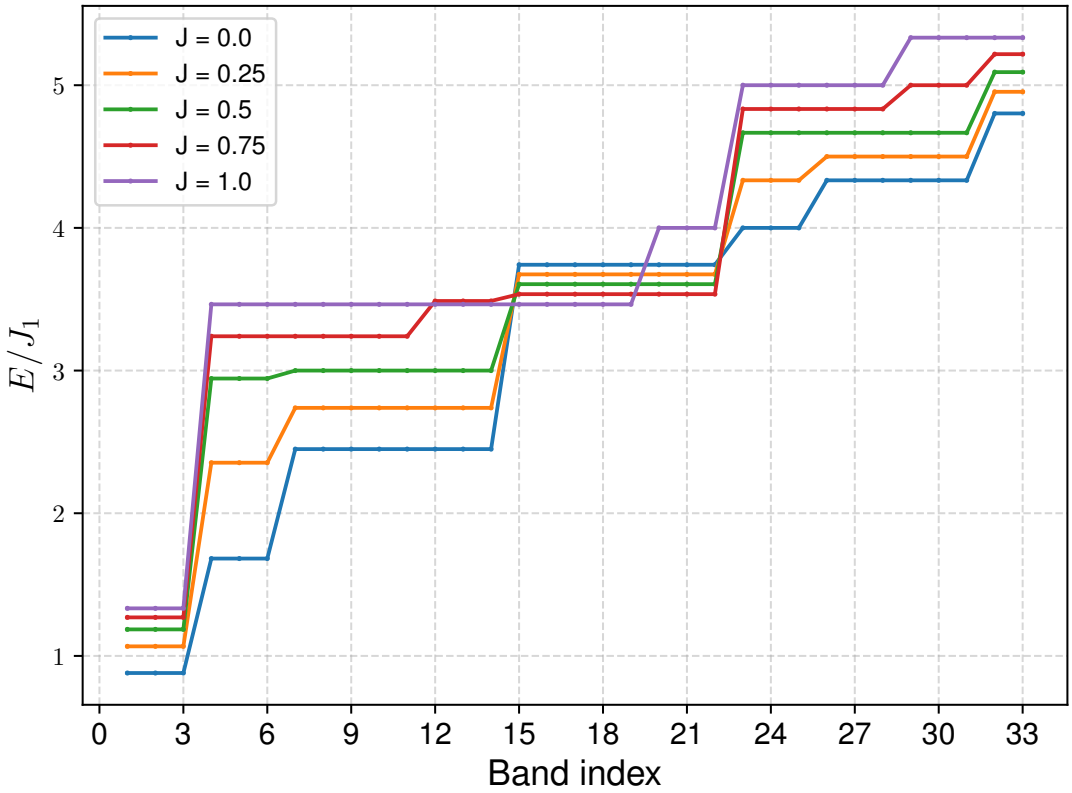

Figure 5.2: Excitation energy of the Trimer phase at the M point as function of band number for different values of $J = J_2/J_1$. Bands are enumerated from lowest excited to highest excited state.

The first qualitative change happens at $J_2/J_1 = 0.75$. Below this value, the second lowest band is 3-fold degenerate, while for $J_2/J_1 = 0.75$ it is 9-fold degenerate. For $J_2/J_1 = 1$, the second lowest band is 16-fold degenerate.

The second qualitative change is level crossing of the twelfth band for $J_2/J_1 = 0.75$ and $J_2/J_1 = 1$.

Looking more closely at the level crossings at the K point, we conduct the same calculation as depicted in Fig. 5.3

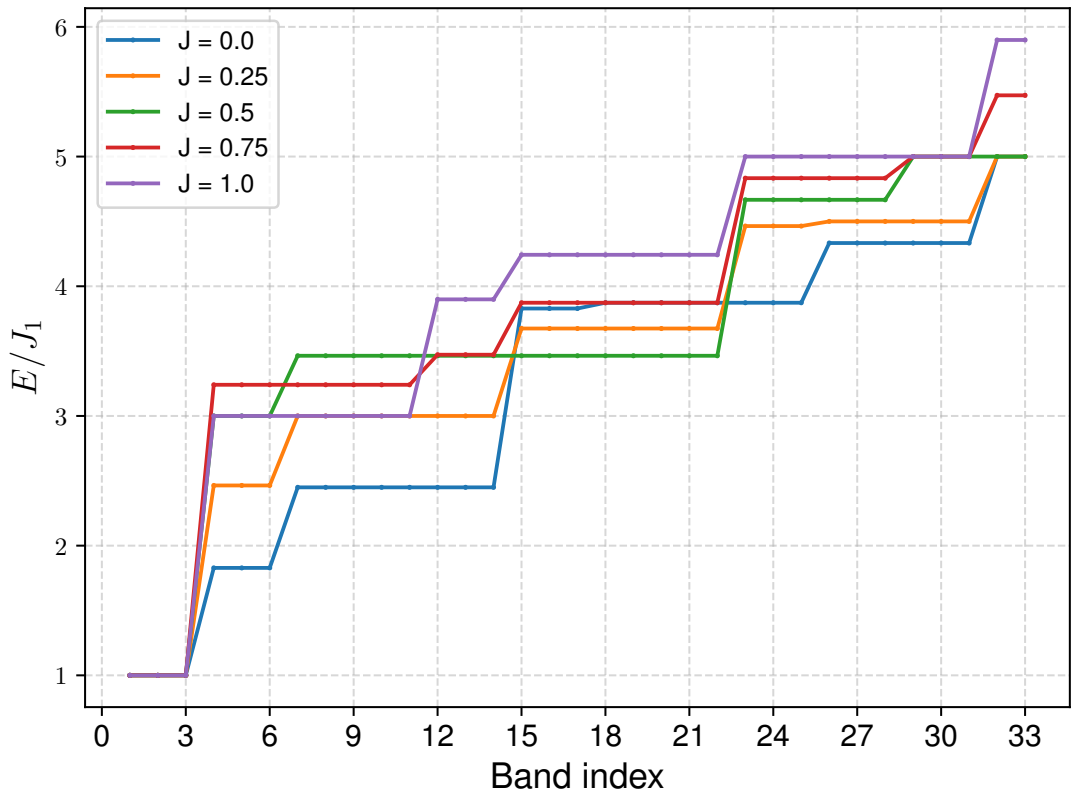

Figure 5.3: Excitation energy of the Triangular phase at the K point as function of band number for different values of $J = J_2/J_1$. Bands are enumerated from lowest excited to highest excited state.

Here, the non-monotonic behavior is shown in the second lowest excitation, between $J_2/J_1 = 0.75$ and $J_2/J_1 = 1$.

5.3 Coupling parameters

Attempting to compare our results to numerical results from (SN: How to cite Inbar's work?), we add two additional parameters changing the coupling strengths.

Focusing on the Trimer phase, we have three distinct types of couplings: triangle-site (AB), on-triangle and inter-triangle (BB). Let

$$\alpha = \frac{\text{Inter-triangle coupling}}{\text{On-triangle coupling}} \tag{5.1}$$

$$\beta = \frac{\text{triangle-site coupling}}{\text{On-triangle coupling}}. \tag{5.2}$$

5.3.1 Scanning of α, β.

Calculation of the fluctuations of the Trimer phase as function of different values of α and β is depicted in Fig. 5.4 and Fig. 5.5

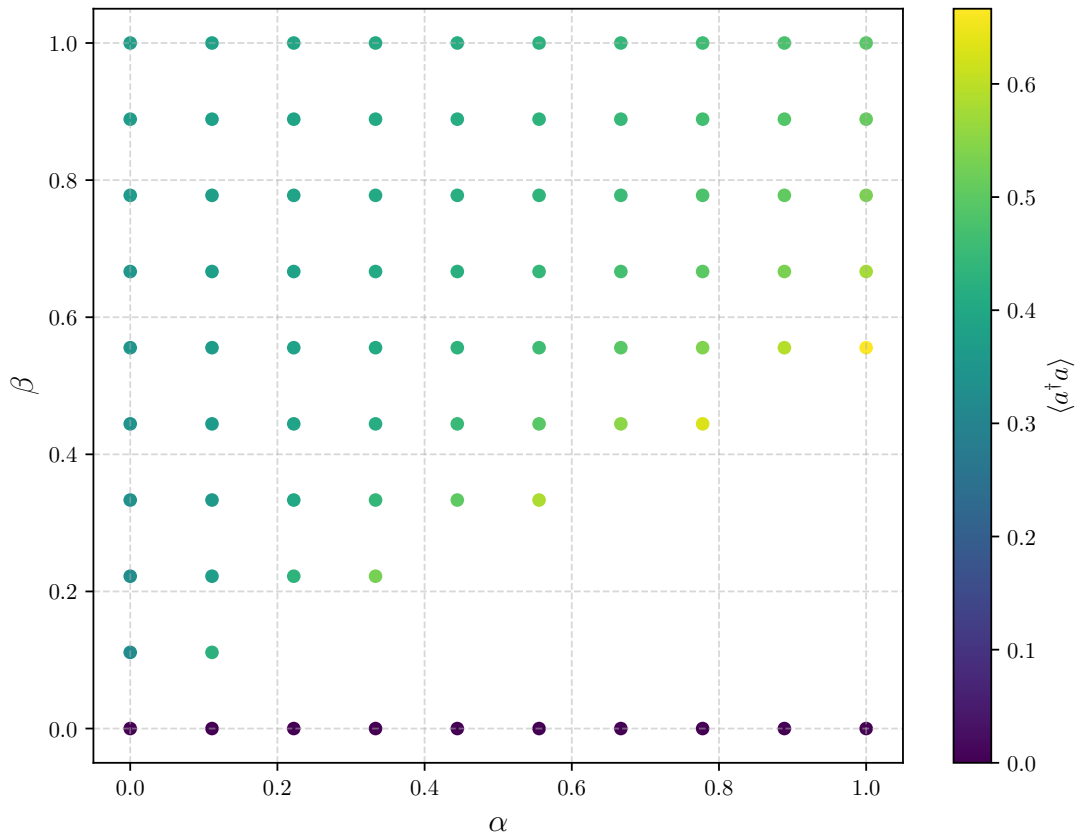

Figure 5.4: Fluctuations on sublattice A as function of α, β of the Trimer phase for $J_2 = 0$.

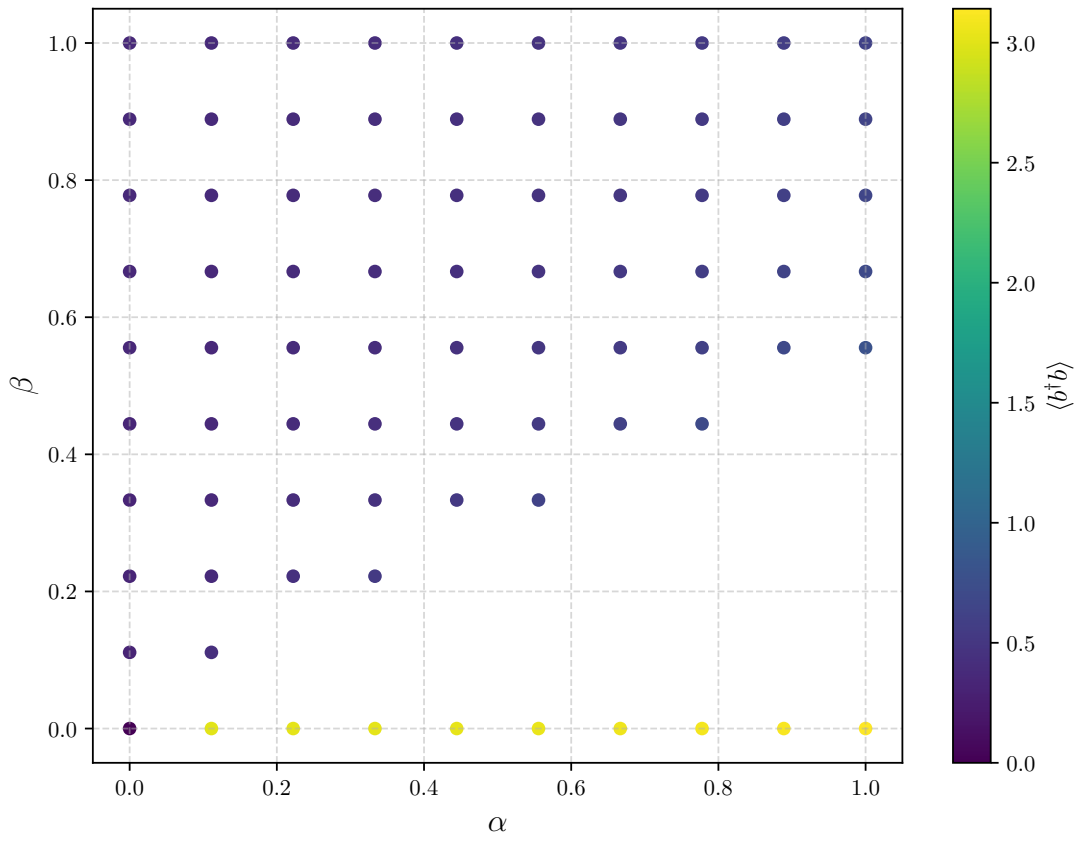

Figure 5.5: Fluctuations on sublattice B as function of α, β of the Trimer phase for $J_2 = 0$.

Missing points on the grid represent points in which the eigenvalues of the Hamiltonian after the Bogoliubov transformation are imaginary. This implies the expansion is invalid when site-trimer couplings are suppressed compared to inter-trimer, apart from a non-analytical behavior as a function of α, β when $\beta = 0$.

5.3.2 Fluctuations Breakdown

Checking the dependency on the ratio of α and β we shall define $\tan\theta = \frac{\beta}{\alpha}$. Scanning the fluctuations on each of the sublattices,

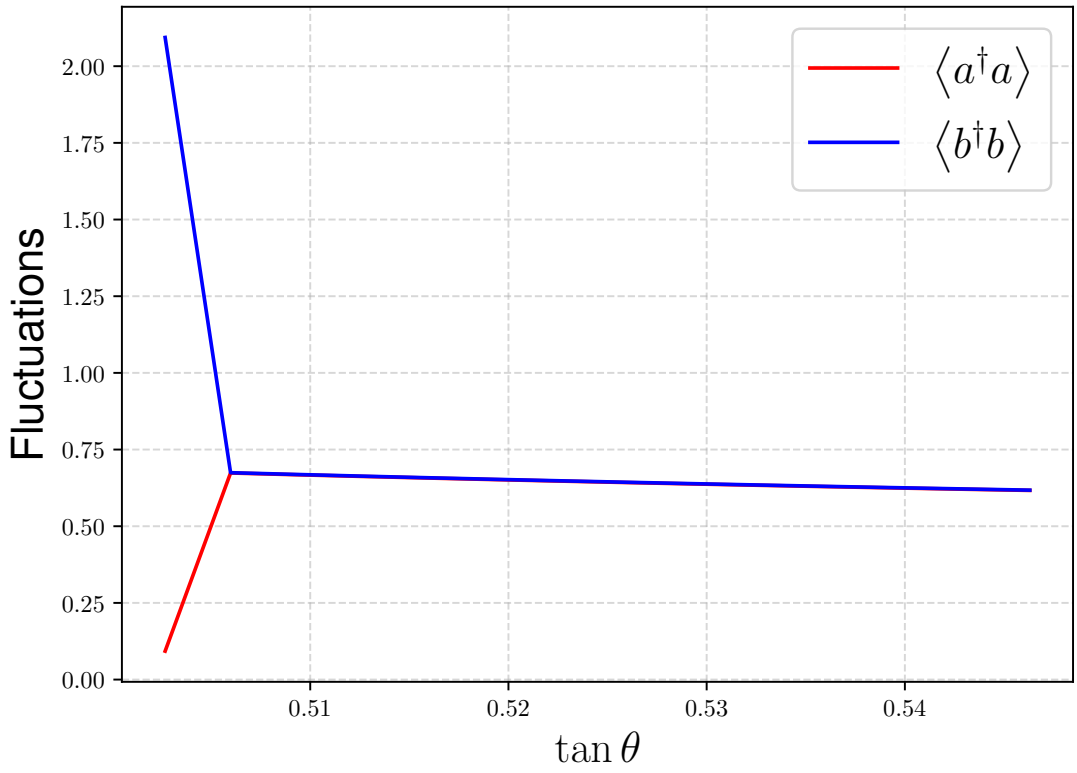

Figure 5.6: For $r = 0.1$ radius

and the HSP

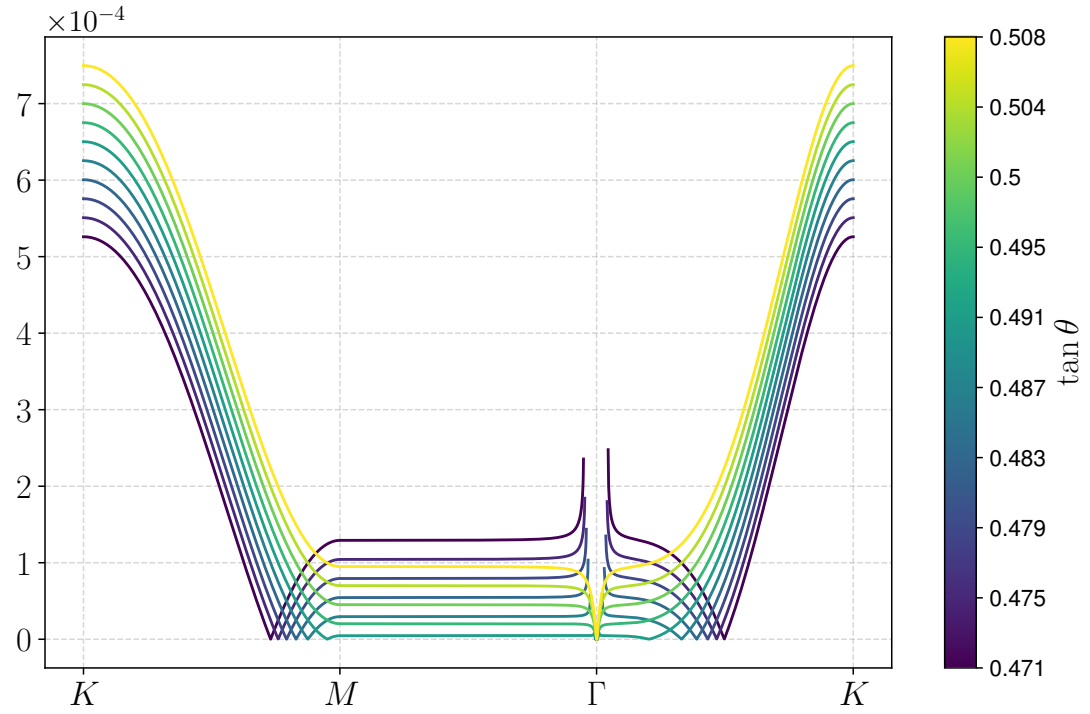

Figure 5.7: Lowest band spectrum on the High Symmetry Path for different values of θ with $r = 0.1$.

Appendix A

Geometry and Bonds

In units of lattice vector length equals 1, we define lattice vectors to be:

$$\vec{a}_1 = \begin{pmatrix} 1 & 0 \end{pmatrix} \tag{A.1}$$

$$\vec{a}_2 = \begin{pmatrix} \cos\frac{2\pi}{3} & \sin\frac{2\pi}{3} \end{pmatrix}. \tag{A.2}$$

The nearest-neighbor and next-nearest-neighbor interactions on a triangular lattice are depicted in Fig. A.1

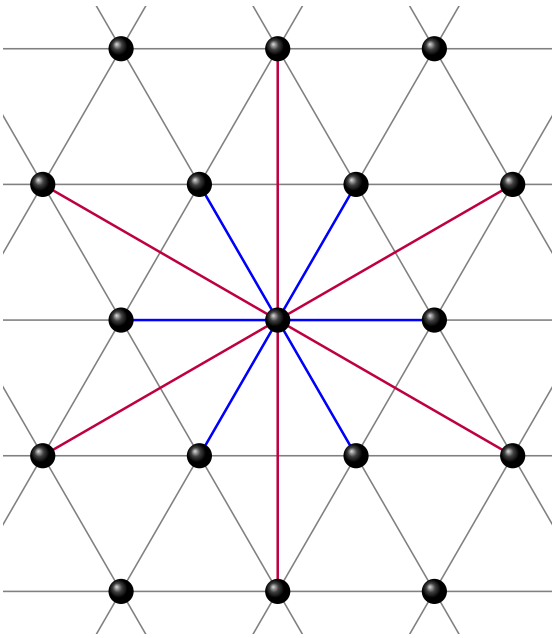

Figure A.1: A single site's nearest-neighbors and next-nearest-neighbors, denoted by connecting lines in blue and purple respectively.

A.1 Néel Bonds

The Néel phase has a four-site parallelogram unit cell. We shall use the notation (i, ℓ) with i parallelogram index and ℓ site within the parallelogram, following the notation

in Fig. 4.2.

Using the point group symmetry and translational symmetry of the triangular lattice, we can define bonds between sites with $\ell_1 < \ell_2$ as $\vec{\chi}_{mn} = -\vec{\chi}_{nm}$. The nearest-neighbor bonds are:

$$\vec{\chi}_{12} = \begin{pmatrix} 1 & 0 \end{pmatrix} \tag{A.3}$$
$$\vec{\chi}_{13} = \begin{pmatrix} \cos\left(\frac{2\pi}{6}\right) & \sin\left(\frac{2\pi}{6}\right) \end{pmatrix} \tag{A.4}$$
$$\vec{\chi}_{14} = \begin{pmatrix} \cos\left(\frac{2\pi}{3}\right) & \sin\left(\frac{2\pi}{3}\right) \end{pmatrix} \tag{A.5}$$
$$\vec{\chi}_{23} = \begin{pmatrix} \cos\left(\frac{2\pi}{3}\right) & \sin\left(\frac{2\pi}{3}\right) \end{pmatrix} \tag{A.6}$$
$$\vec{\chi}_{24} = \begin{pmatrix} \cos\left(\frac{2\pi}{6}\right) & \sin\left(\frac{2\pi}{6}\right) \end{pmatrix} \tag{A.7}$$
$$\vec{\chi}_{34} = \begin{pmatrix} 1 & 0 \end{pmatrix} \tag{A.8}$$

as depicted in Fig. A.2 in colored lines.

The next-nearest-neighbor bonds are

$$\vec{\chi}_{12} = \sqrt{3}\begin{pmatrix} 0 & 1 \end{pmatrix} \tag{A.9}$$
$$\vec{\chi}_{13} = \sqrt{3}\begin{pmatrix} \cos\left(-\frac{2\pi}{6}\right) & \sin\left(-\frac{2\pi}{6}\right) \end{pmatrix} \tag{A.10}$$
$$\vec{\chi}_{14} = \sqrt{3}\begin{pmatrix} \cos\left(\frac{2\pi}{6}\right) & \sin\left(\frac{2\pi}{6}\right) \end{pmatrix} \tag{A.11}$$
$$\vec{\chi}_{23} = \sqrt{3}\begin{pmatrix} \cos\left(\frac{2\pi}{6}\right) & \sin\left(\frac{2\pi}{6}\right) \end{pmatrix} \tag{A.12}$$
$$\vec{\chi}_{24} = \sqrt{3}\begin{pmatrix} \cos\left(-\frac{2\pi}{6}\right) & \sin\left(-\frac{2\pi}{6}\right) \end{pmatrix} \tag{A.13}$$
$$\vec{\chi}_{34} = \sqrt{3}\begin{pmatrix} 0 & 1 \end{pmatrix} \tag{A.14}$$

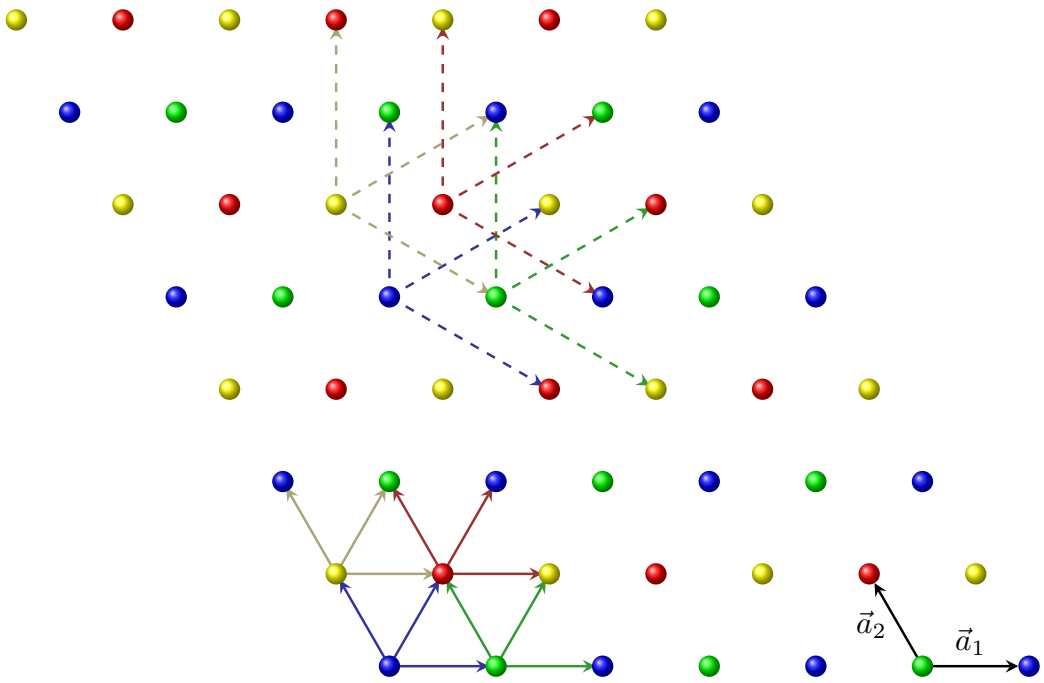

Figure A.2: Visualization of the bonds in the Néel phase. The lattice vectors as defined in Eq. (A.1) and Eq. (A.2) are depicted on the bottom right corner of the figure in black arrows. The nearest-neighbor bonds as defined in Eq. (A.3)-Eq. (A.8) are depicted in colored arrows on the bottom left of the figure. The next-nearest-neighbor bonds as defined in Eq. (A.9)- Eq. (A.14) are depicted in the upper center part of the figure in dashed arrows.

A.2 Trimerized Bonds

We can think of our system as being mapped to the bipartite hexagonal lattice with the single-site representation on sublattice A, and the three-site triangle on sublattice B. This mapping is depicted in Fig. A.3.

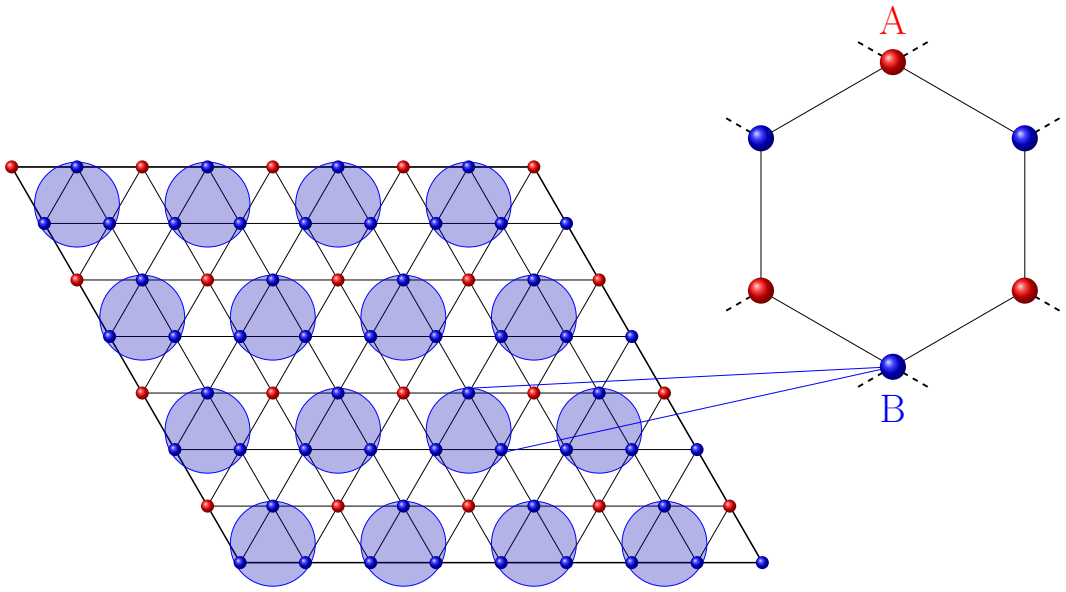

Figure A.3: Mapping of a Trimerized structured triangular lattice to a bipartite hexagonal lattice.

The triangular lattice bonds of the Néel phase with this mapping give bonds between sublattice A and B, and two types of bonds between sublattice B to itself - inter-site and on-site. The bonds within the unit cell are mapped to an on-site interaction with $\vec{\chi} = 0$, and the rest are mapped to inter-site interactions. (SN: Give Hexagonal mapping and define with this the BB and AB bonds.)

Appendix B

Derivation of the Trimerized Flavor-Wave Hamiltonian

Starting from Eq. (3.9) and Eq. (3.10), the full Hamiltonian is $H = H_{AB} + H_{BB}$, with:

$$H_{AB} = \sum_{\substack{i,j \\ \ell\in[3]}} \sum_{\mu\nu} \sum_{m,n} J_{\vec{\chi}} \left(A_\ell^{\mu\nu}\right)_{mn} b^\dagger_{m,i} b_{n,i} a^\dagger_{\nu,j} a_{\mu,j} \tag{B.1}$$

$$H_{BB} = \sum_{\substack{i,j \\ \ell_1,\ell_2\in[3]}} \sum_{\mu\nu} \sum_{\substack{m,n \\ r,s}} J_{\vec{\chi}} \left(A_{\ell_1}^{\mu\nu}\right)_{mn} \left(A_{\ell_2}^{\nu\mu}\right)_{rs} b^\dagger_{m,i} b_{n,i} b^\dagger_{r,j} b_{s,j}. \tag{B.2}$$

We plug in the hard core Bosonic constraints of Eq. (3.11) and Eq. (3.13),

$$a^\dagger_{4,i} a_{4,i} = S - \sum_{\mu\neq 4} a^\dagger_{\mu,i} a_{\mu,i} \tag{B.3}$$

$$b^\dagger_{\bar{4},i} b_{\bar{4},i} = S - \sum_{m\neq\bar{4}} b^\dagger_{m,i} b_{m,i} \tag{B.4}$$

and the large S expansions of Eq. (3.12) and Eq. (3.14),

$$a^\dagger_{4,i}, a_{4,i} \approx \sqrt{S - \sum_{\mu\neq 4} a^\dagger_{\mu,i} a_{\mu,i}} \approx \sqrt{S} \tag{B.5}$$

$$b^\dagger_{\bar{4},i}, b_{\bar{4},i} \approx \sqrt{S - \sum_{m\neq\bar{4}} b^\dagger_{m,i} b_{m,i}} \approx \sqrt{S} \tag{B.6}$$

to derive the Flavor-Wave Hamiltonian. This explicit symmetry breaking differs between the condensed states, that are 4 and $\bar{4}$, and the residual flavors.

In the large S expansion, we drop terms of order $\mathcal{O}(\sqrt{S})$ in the Hamiltonian. Each term in the Hamiltonian contains 4 field operators, and the order of S in each term is determined by the number of field operators in the condensed states.

We separate the analysis into two sections, Sec. B.1 and Sec. B.2 then combine the results to get the full Flavor-Wave Hamiltonian.

In this chapter we already consider only the relevant subspace $\mathcal{D}$, as defined in Sec. 3.3.1, truncating the local Hilbert space only to the part requiring the Bogoliubov transformation.

We define the Fourier transformation of the Bosonic field operators,

$$a_{\mu,i} = \frac{1}{\sqrt{N}} \sum_{\boldsymbol{k}} e^{-i\boldsymbol{k}\cdot\boldsymbol{r}_i} a_{\mu,\boldsymbol{k}} \tag{B.7}$$

$$b_{m,i} = \frac{1}{\sqrt{N}} \sum_{\boldsymbol{k}} e^{-i\boldsymbol{k}\cdot\boldsymbol{r}_i} b_{m,\boldsymbol{k}} \tag{B.8}$$

with N the number of sites on the lattice, and use the notation of Bosonic field operators vectors:

$$\vec{b}_{\boldsymbol{k}} = (b_{m,\boldsymbol{k}})_m \tag{B.9}$$

$$\vec{a}_{\boldsymbol{k}} = (a_{\mu,\boldsymbol{k}})_\mu \tag{B.10}$$

along the derivation, with m, μ indices corresponding to states within the relevant subspace $\mathcal{D}$.

(SN: Think how to justify dropping $S^{3/2}$ terms. Either direct calculation that I am not sure I have, or as this is an extremum point.)

B.1 BB Interactions

In this section, we focus only on H_{BB}. We plug in the hard core Bosonic constraint and large S expansion in state $\bar{4}$ to get the contribution from H_{BB} to the Flavor-Wave Hamiltonian.

We keep track of only quadratic and linear orders of S, corresponding to four or two of the Multi-Boson field operators being in state $\bar{4}$ respectively.

Such terms come from choosing all 4 or two out of the four field operators to be at state $\bar{4}$, corresponding to quadratic and linear order. There are $\binom{4}{2} + \binom{4}{4} = 6 + 1 = 7$ such options. In the linear case, there are two significantly different options: a couple in the same unit cell, and a couple in different unit cells. To distinguish between the two, we break the sum explicitly into cases of the lattice indices such that $i = j$ and $i \neq j$,

$$H_{BB} = H_{BB}^{Intra} + H_{BB}^{Inter} \tag{B.11}$$

B.1.1 Inter-Trimer Interactions

Focusing on interactions between unit cells, the inter-Trimer interactions are

$$H_{BB}^{Inter} = \sum_{i\neq j}\sum_{\ell_1<\ell_2}\sum_{\vec{\chi}} J_{\vec{\chi}} \sum_{\substack{m,n\\r,s}}\sum_{\mu\nu} \left(A_{\ell_1}^{\mu\nu}\right)_{mn}\left(A_{\ell_2}^{\nu\mu}\right)_{rs} b_{m,i}^\dagger b_{n,i} b_{r,j}^\dagger b_{s,j} \tag{B.12}$$

$$\begin{aligned}
\mapsto S\sum_{i\neq j}\sum_{\ell_1<\ell_2}\sum_{\vec{\chi}} J_{\vec{\chi}}\Big[&\sum_{m,s}\sum_{\mu\nu}\left(A_{\ell_1}^{\mu\nu}\right)_{m\bar{4}}\left(A_{\ell_2}^{\nu\mu}\right)_{\bar{4}s} b_{m,i}^\dagger b_{s,j} \\
&+\sum_{n,r}\sum_{\mu,\nu}\left(A_{\ell_1}^{\mu\nu}\right)_{\bar{4}n}\left(A_{\ell_2}^{\nu\mu}\right)_{r\bar{4}} b_{n,i} b_{r,j}^\dagger \\
&+\sum_{m,n}\sum_{\mu,\nu}\left(A_{\ell_1}^{\mu\nu}\right)_{mn}\left(A_{\ell_2}^{\nu\mu}\right)_{\bar{4}\bar{4}} b_{m,i}^\dagger b_{n,i} \\
&+\sum_{r,s}\sum_{\mu,\nu}\left(A_{\ell_1}^{\mu\nu}\right)_{\bar{4}\bar{4}}\left(A_{\ell_2}^{\nu\mu}\right)_{rs} b_{r,j}^\dagger b_{s,j} \\
&+\sum_{n,s}\sum_{\mu,\nu}\left(A_{\ell_1}^{\mu\nu}\right)_{\bar{4}n}\left(A_{\ell_2}^{\nu\mu}\right)_{\bar{4}s} b_{n,i} b_{s,j} \\
&+\sum_{m,r}\sum_{\mu,\nu}\left(A_{\ell_1}^{\mu\nu}\right)_{m\bar{4}}\left(A_{\ell_2}^{\nu\mu}\right)_{r\bar{4}} b_{m,i}^\dagger b_{r,j}^\dagger\Big] \\
&+\left(A_{\ell_1}^{\mu\nu}\right)_{\bar{4}\bar{4}}\left(A_{\ell_2}^{\nu\mu}\right)_{\bar{4}\bar{4}} b_{\bar{4},i}^\dagger b_{\bar{4},i} b_{\bar{4},j}^\dagger b_{\bar{4},j}\Big].
\end{aligned} \tag{B.13}$$

The last line contributes both quadratic and linear orders of S to the expansion as

$$b_{\bar{4},i}^\dagger b_{\bar{4},i} b_{\bar{4},j}^\dagger b_{\bar{4},j} = \left(S - \sum_{m\neq\bar{4}} b_{m,i}^\dagger b_{m,i}\right)\left(S - \sum_{m\neq\bar{4}} b_{m,j}^\dagger b_{m,j}\right) \tag{B.14}$$

$$= S^2 - 2S\sum_{m\neq\bar{4}} b_{m,\boldsymbol{k}}^\dagger b_{m,\boldsymbol{k}} + \mathcal{O}(\sqrt{S}) \tag{B.15}$$

where in the last equation we use Fourier transformation. By taking the Fourier transformation of the rest, collecting terms and using the Bosonic canonical commutation relations, the Flavor-Wave Hamiltonian of the inter-trimer interactions takes the form of:

$$H_{BB}^{\text{Inter}} \approx \mathcal{E}_{\text{BB}}^{\text{Inter}} + \sum_{\boldsymbol{k}>0}\begin{pmatrix}\vec{b}_{\boldsymbol{k}}^\dagger & \vec{b}_{-\boldsymbol{k}}\end{pmatrix}\begin{pmatrix}\mathcal{N}_{\boldsymbol{k},\vec{\chi}}^{\text{Inter}} & \mathcal{A}_{\boldsymbol{k},\vec{\chi}}^{\text{Inter}} \\ \mathcal{A}_{\boldsymbol{k},\vec{\chi}}^{\text{Inter}} & \mathcal{N}_{-\boldsymbol{k},\vec{\chi}}^{\text{Inter}}\end{pmatrix}\begin{pmatrix}\vec{b}_{\boldsymbol{k}} \\ \vec{b}_{-\boldsymbol{k}}^\dagger\end{pmatrix}. \tag{B.16}$$

with

$$\left(\mathcal{A}^{\text{Inter}}_{\boldsymbol{k},\vec{\chi}}\right)_{i,j} = \sum_{\ell_1<\ell_2}\sum_{\vec{\chi}}\sum_{\mu,\nu} SJ_{\vec{\chi}}\left[\left(A^{\mu\nu}_{\ell_1}\right)_{i,\bar{4}}\left(A^{\nu\mu}_{\ell_2}\right)_{j,\bar{4}} e^{-i\boldsymbol{k}\cdot\vec{\chi}} + \text{h.c}\right] \tag{B.17}$$

$$\left(\mathcal{N}^{\text{Inter}}_{\boldsymbol{k},\vec{\chi}}\right)_{i,j} = \left(\mathcal{C}^{N}_{\boldsymbol{k},\vec{\chi}} + \mathcal{C}^{L}\right)_{i,j} \tag{B.18}$$

$$\left(\mathcal{C}^{N}_{\boldsymbol{k},\vec{\chi}}\right)_{i,j} = \sum_{\ell_1<\ell_2}\sum_{\vec{\chi}}\sum_{\mu,\nu} SJ_{\vec{\chi}}\left[\left(A^{\mu\nu}_{\ell_1}\right)_{i,\bar{4}}\left(A^{\nu\mu}_{\ell_2}\right)_{\bar{4},j} e^{-i\boldsymbol{k}\cdot\vec{\chi}} + \text{h.c}\right] \tag{B.19}$$

$$\begin{aligned}\left(\mathcal{C}^{L}\right)_{i,j} = \sum_{\ell_1<\ell_2}\sum_{\vec{\chi}}\sum_{\mu,\nu} SJ_{\vec{\chi}}\Big[&\left(A^{\mu\nu}_{\ell_1}\right)_{\bar{4},\bar{4}}\left(A^{\nu\mu}_{\ell_2}\right)_{i,j} + \left(A^{\mu\nu}_{\ell_1}\right)_{i,j}\left(A^{\nu\mu}_{\ell_2}\right)_{\bar{4},\bar{4}} \\ &- 2\left(A^{\mu\nu}_{\ell_1}\right)_{\bar{4},\bar{4}}\left(A^{\nu\mu}_{\ell_2}\right)_{\bar{4},\bar{4}}\delta_{ij}\Big]\end{aligned} \tag{B.20}$$

$$\mathcal{E}^{\text{Inter}}_{\text{BB}} = -\frac{1}{2}\sum_{\boldsymbol{k}\neq 0} Tr\left[\mathcal{C}^{L}\right] + S^2\sum_{\boldsymbol{k}}\sum_{\ell_1<\ell_2}\sum_{\mu\nu}\sum_{\vec{\chi}} J_{\vec{\chi}}\left(A^{\mu\nu}_{\ell_1}\right)_{\bar{4}\bar{4}}\left(A^{\nu\mu}_{\ell_2}\right)_{\bar{4}\bar{4}} \tag{B.21}$$

with the sum over $\vec{\chi}$ following the derivation of the BB bonds in Chapter A.

B.1.2 Intra-Trimer Interactions

Focusing on the intra-Trimer interactions only, the part of H^{L}_{BB} is a Hamiltonian of decoupled Trimers. Moreover, as the Multi-Bosons are not localized on a specific site within the unit cell, we get an effective on-site interaction.

As in conventional Holstein-Primakoff approximations there are no on-site interactions, we check for the validity of Flavor-Wave approximations on these terms.

This decoupled structure gives a seperable Hamiltonian:

$$H^{\text{Intra}}_{\text{BB}} = \sum_{\substack{i\\ \ell_1,\ell_2\in[3]}}\sum_{\mu\nu}\sum_{\substack{m,n\\ r,s}} J_{\vec{\chi}}\left(A^{\mu\nu}_{\ell_1}\right)_{mn}\left(A^{\nu\mu}_{\ell_2}\right)_{rs} b^{\dagger}_{m,i}b_{n,i}b^{\dagger}_{r,i}b_{s,i} \tag{B.22}$$

which is a direct sum of 64 dimensional Hamiltonians. They are diagonalized exactly in the $SU(4)$ irreducible basis, giving the diagonalized form,

$$H^{\text{Intra}}_{\text{BB}} = \sum_{i}\sum_{m=1}^{64}\varepsilon_m b^{\dagger}_{m,i}b_{m,i} = \sum_{\boldsymbol{k}}\sum_{m=1}^{64}\varepsilon_m b^{\dagger}_{m,\boldsymbol{k}}b_{m,\boldsymbol{k}} \tag{B.23}$$

with

$$\varepsilon_m = \begin{cases} -3J_1 & m\in AS \\ 0 & m\in M \\ 3J_1 & m\in S \end{cases} \tag{B.24}$$

with AS, M and S notations of the fully anti-symmetric (anti-fundamental), mixed, and fully symmetric (fundamental) representations of $SU(4)$.

We compare this result with a Flavor-Wave approximation on this Hamiltonian, and

find the dispersion completely different (SN: Think if to add the dispersion from the Flavor-Wave expansion), indicating the invalidity of this approximation on this part of the Hamiltonian. Therefore, we use the exact diagonalization of these terms before conducting the Flavor-Wave approximation on them. Continuing from Eq. (B.23), we restore orders of S by using the fact that $S = 1$, and by so we get:

$$H_{BB}^{Intra} = J_1 \sum_{\boldsymbol{k}} \left(3 \sum_{a \in S} b_{a,\boldsymbol{k}}^\dagger b_{a,\boldsymbol{k}} - 3 \sum_{a \in AS} b_{a,\boldsymbol{k}}^\dagger b_{a,\boldsymbol{k}} \right) \tag{B.25}$$

$$= J_1 \sum_{\boldsymbol{k}} \left(3 \sum_{a \in S} b_{a,\boldsymbol{k}}^\dagger b_{a,\boldsymbol{k}} - 3 \left(S - \sum_{\ell \neq \bar{4}} b_{\ell,\boldsymbol{k}}^\dagger b_{\ell,\boldsymbol{k}} + \sum_{a \in AS \setminus \bar{4}} b_{a,\boldsymbol{k}}^\dagger b_{a,\boldsymbol{k}} \right) \right) S \tag{B.26}$$

$$= J_1 S \sum_{\boldsymbol{k}} \left(6 \sum_{a \in S} b_{a,\boldsymbol{k}}^\dagger b_{a,\boldsymbol{k}} + 3 \sum_{a \in M} b_{a,\boldsymbol{k}}^\dagger b_{a,\boldsymbol{k}} - 3S \right) \tag{B.27}$$

Using the Bosonic vector notations, we can write this Hamiltonian in matrix form:

$$H_{\mathrm{BB}}^{\mathrm{Intra}} = \sum_{\boldsymbol{k}} \left(-3 J_1 S^2 \right) + J_1 S \sum_{\boldsymbol{k}>0} \begin{pmatrix} \vec{b}_{\boldsymbol{k}}^\dagger & \vec{b}_{-\boldsymbol{k}} \end{pmatrix} E_{\boldsymbol{k}}^{\mathrm{Intra}} \begin{pmatrix} \vec{b}_{\boldsymbol{k}} \\ \vec{b}_{-\boldsymbol{k}}^\dagger \end{pmatrix} \tag{B.28}$$

with

$$\left(E_{\boldsymbol{k}}^{\mathrm{Intra}} \right)_{mn} = \delta_{mn} \cdot \begin{cases} 6 & m \in S \\ 3 & m \in M \\ 0 & m \in AS \end{cases} \tag{B.29}$$

B.1.3 Total BB Hamiltonian

The total Flavor-Wave Hamiltonian of H_{BB} is the sum of Eq. (B.16) and Eq. (B.28), that is written in matrix form,

$$H_{BB} \approx \mathcal{E}_{BB} + \sum_{\boldsymbol{k}>0} \begin{pmatrix} \vec{b}_{\boldsymbol{k}}^\dagger & \vec{b}_{-\boldsymbol{k}} \end{pmatrix} \begin{pmatrix} \mathcal{N}_{\boldsymbol{k},\vec{\chi}}^{\mathrm{Inter}} + E_{\boldsymbol{k}}^{\mathrm{Intra}} & \mathcal{A}_{\boldsymbol{k},\vec{\chi}}^{\mathrm{Inter}} \\ \mathcal{A}_{\boldsymbol{k},\vec{\chi}}^{\mathrm{Inter}} & \left(\mathcal{N}_{\boldsymbol{k},\vec{\chi}}^{\mathrm{Inter}} \right)^* + E_{\boldsymbol{k}}^{\mathrm{Intra}} \end{pmatrix} \begin{pmatrix} \vec{b}_{\boldsymbol{k}} \\ \vec{b}_{-\boldsymbol{k}}^\dagger \end{pmatrix} \tag{B.30}$$

with the Bosonic field operators vector as defined in Eq. (B.9), and

$$\mathcal{E}_{BB} = \sum_{\boldsymbol{k}} \left(-45 J_1 S - 2S^2 \left(J_1 - J_2 \right) - \frac{1}{2} Tr \left[\mathcal{C}^L \right] \right) \tag{B.31}$$

is a term independent of the field operators, contributing to the vacuum state energy.

B.2 AB Interactions

In this section, we plug in the condensate states in H_{AB} and employ the large S expansion. As each term is composed of two Multi-Bosons and two Schwinger-Bosons

field operators, its order of S is determined by the number of flavor indices in the condensed state. The Multi-Boson (Schwinger-Boson) flavor index corresponds to the m, n (μ, ν) indices in the sum.

The quadratic order in S comes from terms in the sum with $\mu = \nu = 4$ and $m = n = \bar{4}$. The expression is as such:

$$H^Q_{AB} = \sum_{i,j} \sum_{\ell=1}^{3} J_{\vec{\chi}} \left(A^{44}\right)_{\bar{4}\bar{4}} \left(S - \sum_{m \neq \bar{4}} b^\dagger_{m,i} b_{m,i}\right) \left(S - \sum_{\mu \neq 4} a^\dagger_{\mu,j} a_{\mu,j}\right). \tag{B.32}$$

From direct calculations, $(A^{44})_{\bar{4}\bar{4}} = 0$. This implies the whole term is 0.

To find linear order in S, we first break the flavor indices,

$$\begin{aligned} H_{AB} = \sum_{i,j} \sum_{\ell=1}^{3} \sum_{m,n} J_{\vec{\chi}} \Big[\sum_{\mu \in [3]} \Big(\left(A^{4\mu}_\ell\right)_{mn} b^\dagger_{m,i} b_{n,i} a^\dagger_{\mu,j} a_{4,j} + \left(A^{\mu 4}_\ell\right)_{mn} b^\dagger_{m,i} b_{n,i} a^\dagger_{4,j} a_{\mu,j} \Big) \\ + \left(A^{44}_\ell\right)_{mn} b^\dagger_{m,i} b_{n,i} a^\dagger_{4,j} a_{4,j} + \sum_{\mu,\nu \in [3]} \left(A^{\mu\nu}_\ell\right)_{mn} b^\dagger_{m,i} b_{n,i} a^\dagger_{\nu,j} a_{\mu,j} \Big] \end{aligned} \tag{B.33}$$

then plugging in the condensates:

$$\begin{aligned} H_{AB} = S \sum_{i,j} \sum_{\ell=1}^{3} J_{\vec{\chi}} \Big[\sum_{\mu \in [3]} \sum_{m \neq \bar{4}} \Big(\left(A^{4\mu}_\ell\right)_{m\bar{4}} b^\dagger_{m,i} a^\dagger_{\mu,j} + \left(A^{\mu 4}_\ell\right)_{m\bar{4}} b^\dagger_{m,i} a_{\mu,j} \\ + \left(A^{4\mu}_\ell\right)_{\bar{4}m} b_{m,i} a^\dagger_{\mu,j} + \left(A^{\mu 4}_\ell\right)_{\bar{4}m} b_{m,i} a_{\mu,j} \Big) \\ + \sum_{m,n \neq \bar{4}} \left(A^{44}_\ell\right)_{mn} b^\dagger_{m,i} b_{n,i} + \sum_{\mu,\nu \in [3]} \left(A^{\mu\nu}_\ell\right)_{\bar{4}\bar{4}} a^\dagger_{\nu,j} a_{\mu,j} \Big]. \end{aligned} \tag{B.34}$$

Taking the Fourier transformation, collecting terms and using the Bosonic canonical commutation relations, we write the Hamiltonian using the concatenated field operators vector $\begin{pmatrix} \vec{b}_{\boldsymbol{k}} & \vec{a}_{\boldsymbol{k}} & \vec{b}^\dagger_{-\boldsymbol{k}} & \vec{a}^\dagger_{-\boldsymbol{k}} \end{pmatrix}^T$:

$$H_{AB} \approx \mathcal{E}_{AB} + \sum_{\boldsymbol{k} > 0} \begin{pmatrix} \vec{b}^\dagger_{\boldsymbol{k}} & \vec{a}^\dagger_{\boldsymbol{k}} & \vec{b}_{-\boldsymbol{k}} & \vec{a}_{-\boldsymbol{k}} \end{pmatrix} \begin{pmatrix} \mathcal{N}^{\mathrm{AB}}_{\boldsymbol{k},\vec{\chi}} & \mathcal{A}^{\mathrm{AB}}_{\boldsymbol{k},\vec{\chi}} \\ \mathcal{A}^{\mathrm{AB}}_{\boldsymbol{k},\vec{\chi}} & \mathcal{N}^{\mathrm{AB}}_{-\boldsymbol{k},\vec{\chi}} \end{pmatrix} \begin{pmatrix} \vec{b}_{\boldsymbol{k}} \\ \vec{a}_{\boldsymbol{k}} \\ \vec{b}^\dagger_{-\boldsymbol{k}} \\ \vec{a}^\dagger_{-\boldsymbol{k}} \end{pmatrix}. \tag{B.35}$$

with $\mathcal{N}^{\mathrm{AB}}_{\boldsymbol{k},\vec{\chi}}, \mathcal{A}^{\mathrm{AB}}_{\boldsymbol{k},\vec{\chi}}$ complex matrices and $\mathcal{E}_{AB}$ a real number. Defining these matrices, we distinguish between terms coupling of Multi-Bosons and Schwinger-Bosons field operators with Latin indices (m, n) referring to Multi-Bosons, and Greek indices (μ, ν)

referring to Schwinger-Bosons. With this notation, the matrix elements are:

$$\left(\mathcal{N}^{\mathrm{AB}}_{\boldsymbol{k},\vec{\chi}}\right)_{mn} = S\sum_{\ell=1}^{3}\sum_{\vec{\chi}} J_{\vec{\chi}}\left(A^{44}_{\ell}\right)_{mn} \tag{B.36}$$

$$\left(\mathcal{N}^{\mathrm{AB}}_{\boldsymbol{k},\vec{\chi}}\right)_{\mu\nu} = S\sum_{\ell=1}^{3}\sum_{\vec{\chi}} J_{\vec{\chi}}\left(A^{\mu\nu}_{\ell}\right)_{\bar{4}\bar{4}} \tag{B.37}$$

$$\left(\mathcal{N}^{\mathrm{AB}}_{\boldsymbol{k},\vec{\chi}}\right)_{m\mu} = S\sum_{\ell=1}^{3}\sum_{\vec{\chi}} J_{\vec{\chi}} e^{-i\boldsymbol{k}\cdot\vec{\chi}}\left(A^{\mu 4}_{\ell}\right)_{m\bar{4}} \tag{B.38}$$

$$\left(\mathcal{A}^{\mathrm{AB}}_{\boldsymbol{k},\vec{\chi}}\right)_{m\mu} = S\sum_{\ell=1}^{3}\sum_{\vec{\chi}} J_{\vec{\chi}} e^{-i\boldsymbol{k}\cdot\vec{\chi}}\left(A^{4\mu}_{\ell}\right)_{m\bar{4}} \tag{B.39}$$

$$\left(\mathcal{A}^{\mathrm{AB}}_{\boldsymbol{k},\vec{\chi}}\right)_{mn} = \left(\mathcal{A}^{\mathrm{AB}}_{\boldsymbol{k},\vec{\chi}}\right)_{\mu\nu} = 0 \tag{B.40}$$

$$\mathcal{E}_{\mathrm{AB}} = -S\sum_{\boldsymbol{k}}\sum_{\ell=1}^{3}\left(J_1 + J_2\right)\left(1 + Tr\left[A^{44}_{\ell}\right]\right) \tag{B.41}$$

with the sum over $\vec{\chi}$ following the derivation of the AB bonds in Chapter A.

B.3 Vacuum State Energy

The vacuum state energy of the Trimerized phase comes from the constant terms (independent of the field operators) in the diagonalized Hamiltonian. Such terms come both from the constant terms in Eq. (B.30) and Eq. (B.35), and from the constant terms of the Bogoliubov transformation as described in Sec. 2.5.1.

The constant term from the Bogoliubov transformation is

$$\mathcal{E}_{Bog} = S\sum_{\boldsymbol{k}}\sum_{m\in\mathcal{D}}\frac{1}{2}\omega_{m,\boldsymbol{k}} \tag{B.42}$$

with $\omega_{m,\boldsymbol{k}}$ the dispersion.

Therefore, using Eq. (B.31), Eq. (B.41) and Eq. (B.42) the total Trimerized phase's vacuum state energy is

$$\mathcal{E} = \mathcal{E}_{BB} + \mathcal{E}_{AB} + \mathcal{E}_{Bog}. \tag{B.43}$$

Appendix C

Derivation of the Néel Flavor Wave Hamiltonian

Appendix D

Fluctuations

In this chapter, we calculate the fluctuations on each of the sublattices in the Trimerized vacuum state, as defined in Eq. (3.22) and Eq. (3.23).

D.1 Relevant Subspace

Following Sec. 2.7, the exclusion principles dictate the Hamiltonian, being $SU(3)$ symmetric in the Trimerized phase, breaks to a direct sum of a subspace having anomalous terms and a subspace that does not. We shall refer to the subspace with anomalous terms as the relevant subspace.

As the irrelevant subspace, i.e the completion of the relevant subspace, does not contain any anomalous terms, it is diagonalizable unitarily. As the vacuum state is invariant under unitary transformations, the fluctuations are unaffected by this subspace.

By direct calculations, the relevant subspace is 34 dimensional, with 31 states from the Multi-Bosons field operators defined on sublattice B and 3 Schwinger-Bosons defined on sublattice A. (SN: Check if this is true as we work not in the irrep. basis of $SU(3)$. There might be less states.)

D.2 Field Operators

Let the Schwinger-Bosons field operators on sublattice A, $\vec{a}_{\boldsymbol{k}} = (a_{\mu,\boldsymbol{k}})_{\mu=1}^{3}$, and the relevant Multi-Bosons field operators on sublattice B in the irreducible representation basis $\vec{b}_{\boldsymbol{k}} = (b_{m,,\boldsymbol{k}})_{m=1}^{63}$ with $\mu = 4$ and $m = 64$ corresponding to the condensed flavor 4 and $\bar{4}$ respectively (Sec. 3.3.

Let the concatenated vector of field operators:

$$\vec{\zeta}_{\boldsymbol{k}} = \begin{pmatrix} \vec{b}_{\boldsymbol{k}} \\ \vec{a}_{\boldsymbol{k}} \\ \vec{b}^{\dagger}_{-\boldsymbol{k}} \\ \vec{a}^{\dagger}_{-\boldsymbol{k}} \end{pmatrix}. \tag{D.1}$$

Let the field operators after the Bogoliubov transformation (Sec. 2.5) $(\alpha_{n,\boldsymbol{k}})_{n=1}^{66}$. They satisfy the Bosonic commutation relations:

$$\left[\alpha_{m,\boldsymbol{k}}, \alpha^{\dagger}_{n,\boldsymbol{k}'}\right] = \delta_{m,n}\delta\left(\boldsymbol{k} - \boldsymbol{k}'\right) \tag{D.2}$$

and are obtained via the transformation matrix $W_{\boldsymbol{k}}$ satisfying:

$$\vec{\zeta}_{\boldsymbol{k}} = W_{\boldsymbol{k}}\vec{\xi}_{\boldsymbol{k}} \tag{D.3}$$

with

$$\vec{\xi}_{\boldsymbol{k}} = \begin{pmatrix} \vec{\alpha}_{\boldsymbol{k}} \\ \vec{\alpha}^{\dagger}_{-\boldsymbol{k}} \end{pmatrix} \tag{D.4}$$

We write $W_{\boldsymbol{k}}$ in a block formation, corresponding to the different subspaces as depicted in Fig. 3.4,

$$W_{\boldsymbol{k}} = \begin{pmatrix} U_{\boldsymbol{k}} & V_{\boldsymbol{k}} \\ V^{T}_{-\boldsymbol{k}} & U_{-\boldsymbol{k}} \end{pmatrix} \tag{D.5}$$

with $U_{\boldsymbol{k}}, V_{\boldsymbol{k}} \in \mathbb{C}^{66\times 66}$ and $W_{\boldsymbol{k}}$ is obtained as the eigenvector matrix, that diagonalizes the Hamiltonian.

Therefore, the field operators obey

$$a_{\ell,\boldsymbol{k}} = \sum_{m=1}^{66} (U_{\boldsymbol{k}})_{63+\ell,m}\, \alpha_{m,\boldsymbol{k}} + \sum_{m=1}^{66} (V_{\boldsymbol{k}})_{63+\ell,m}\, \alpha^{\dagger}_{m,-\boldsymbol{k}} \tag{D.6}$$

$$a^{\dagger}_{\ell,\boldsymbol{k}} = \sum_{m=1}^{66} (U_{\boldsymbol{k}})^{*}_{63+\ell,m}\, \alpha^{\dagger}_{m,\boldsymbol{k}} + \sum_{m=1}^{66} (V_{\boldsymbol{k}})^{*}_{63+\ell,m}\, \alpha_{m,-\boldsymbol{k}} \tag{D.7}$$

$$b_{\ell,\boldsymbol{k}} = \sum_{m=1}^{66} (U_{\boldsymbol{k}})_{\ell,m}\, \alpha_{m,\boldsymbol{k}} + \sum_{m=1}^{66} (V_{\boldsymbol{k}})_{\ell,m}\, \alpha^{\dagger}_{m,-\boldsymbol{k}} \tag{D.8}$$

$$b^{\dagger}_{\ell,\boldsymbol{k}} = \sum_{m=1}^{66} (U_{\boldsymbol{k}})^{*}_{\ell,m}\, \alpha^{\dagger}_{m,\boldsymbol{k}} + \sum_{m=1}^{66} (V_{\boldsymbol{k}})^{*}_{\ell,m}\, \alpha_{m,-\boldsymbol{k}} \tag{D.9}$$

In addition, from the vacuum state's definition, as it is the vacuum of the $\alpha_{n,\boldsymbol{k}}$

operators,

$$\forall n, \boldsymbol{k} \qquad \alpha_{n,\boldsymbol{k}} |0\rangle = 0 \tag{D.10}$$

D.3 Calculating the Fluctuations

Plugging Eq. (D.6) - Eq. (D.9) and Eq. (D.10) in Eq. (3.22), the fluctuations on sublattice A are:

$$\langle a^\dagger a \rangle = \frac{1}{N} \sum_{\boldsymbol{k}} \sum_{\ell=1}^{3} \langle a^\dagger_{\ell,\boldsymbol{k}} a_{\ell,\boldsymbol{k}} \rangle \tag{D.11}$$

$$= \frac{1}{N} \sum_{\boldsymbol{k}} \sum_{\ell=1}^{3} \sum_{m=1}^{66} \left| (V_{\boldsymbol{k}})_{63+\ell,m} \right|^2 \tag{D.12}$$

and the fluctuations on sublattice B are:

$$\langle b^\dagger b \rangle = \frac{1}{N} \sum_{\boldsymbol{k}} \sum_{\ell=1}^{63} \langle b^\dagger_{\ell,\boldsymbol{k}} b_{\ell,\boldsymbol{k}} \rangle \tag{D.13}$$

$$= \frac{1}{N} \sum_{\boldsymbol{k}} \sum_{\ell=1}^{63} \sum_{m=1}^{66} \left| (V_{\boldsymbol{k}})_{\ell,m} \right|^2 . \tag{D.14}$$

Bibliography

[1] Alexey Vyacheslavovich Gorshkov, M Hermele, V Gurarie, C Xu, Paul S Julienne, J Ye, Peter Zoller, Eugene Demler, Mikhail D Lukin, and AM Rey. Two-orbital su (n) magnetism with ultracold alkaline-earth atoms. *Nature physics*, 6(4):289–295, 2010.

[2] Hui-Ke Jin, Rong-Yang Sun, Hong-Hao Tu, and Yi Zhou. Unveiling a critical stripy state in the triangular-lattice su (4) spin-orbital model. *Science Bulletin*, 67(9):918–923, 2022.

[3] K. I. Kugel and D. I. Khomskii. The jahn-teller effect and magnetism: transition metal compounds. *Soviet Physics Uspekhi*, 25(4):231–256, 1982.

[4] Kliment I Kugel and Daniel I Khomskii. Crystal-structure and magnetic properties of substances with orbital degeneracy. *Zh. Eksp. Teor. Fiz*, 64:1429–1439, 1973.

[5] N David Mermin and Herbert Wagner. Absence of ferromagnetism or antiferromagnetism in one-or two-dimensional isotropic heisenberg models. *Physical Review Letters*, 17(22):1133, 1966.

[6] Karlo Penc, Matthieu Mambrini, Patrik Fazekas, and Frédéric Mila. Quantum phase transition in the SU(4) spin-orbital model on the triangular lattice. *Phys. Rev. B*, 68:012408, Jul 2003.

[7] Andrew Smerald and Frédéric Mila. Exploring the spin-orbital ground state of ba 3 cusb 2 o 9. *Physical Review B*, 90(9):094422, 2014.

[8] Vladimir Kalnitsky, Inbar Kazas et al. Ground state of the SU(4) Heisenberg antiferromagnet on a triangular lattice. *In preperation*, 2025.

[9] Masahiko G Yamada, Masaki Oshikawa, and George Jackeli. Emergent su (4) symmetry in α-zrcl 3 and crystalline spin-orbital liquids. *Physical Review Letters*, 121(9):097201, 2018.

המוחלט (0 קלווין), הטריונים הם יציבים יחסית ומקיימים קורלציות דמויות ארוכות טווח. תוצאה זו מספקת תובנות חדשות על הדינמיקה של הטריונים ועל אופני הפיזור שלהם במערכות חד ממדיות, אשר עשויות להיות רלוונטיות גם למחקרים על חומרים דו ממדיים.

המשך מתבקש לעבודת המחקר הנוכחי היא יישום של דרגות חופש נוספות, כמו דרגת חופש של ספין האלקטרון, שעשויה לספק תיקונים במבנה הספקטרלי עבור מדידות במעבדה בשל משקל ספקטרלי סופי למדידת מצבים טריוניים בעלי תנע סריג אפס במצב האנטי-סימטרי (ספין $1/2$). המשך נוסף קשור למעבר פאזה מבני אליו לא התייחסנו, השובר סימטריה גיאומטרית של שיקוף השרשרת החד מימדית ומאפשר את עיבוי האקסיטונים.

המחקר המתואר בעבודה זו תורם להבנת הפיסיקה של פאזה מבודדת אקסיטונית, חוקר את התנאים הנדרשים להיווצרות טריונים, ומציע דרכים ניסיוניות לזיהוי פאזה זו. מסקנות המחקר צפויות להיות רלוונטיות למגוון תחומים, החל ממדעי החומר ועד לטכנולוגיות עתידיות המבוססות על הולכה טריונית ומניפולציה של אינטראקציות אלקטרוניות בחומרים קוונטיים. המחקר פותח כיווני מחקר חדשים להבנת תופעות קולקטיביות בקנה מידה ננומטרי.

מלאכותית נקייה מפגמים ומרעשים ועם שליטה גבוה בפרמטרים של הבעיה. דבר זה מאפשר בידוד מוצלח של דרגות החופש הרלוונטיות לבעיה. לצד היכולת המתוחכמת לספק הסברים לתצפיות ניסיוניות, הדבר מאפשר גם סיפוק של תחזיות ופותח רעיונות לניסויים עתידיים, כפי שנספק במחקר הנוכחי.

שימוש בשיטות חישוביות מתקדמות, כגון אלגוריתם חבורת הרנורמליזציה של מטריצת הצפיפות (DMRG) ולכסון מדויק (ED), מאפשר לנו למצוא את מצב היסוד הקוונטי של מערכת מרובת גופים. בעזרת ערכי התצפית של המערכת, התאפשר מיפוי של דיאגרמת הפאזות וזיהוי את התנאים שבהם מתקיימת פאזה טריונית יציבה, כתלות בחוזק האינטראקציה ובפער האנרגיה בין פס ההולכה לפס הערכיות. שימוש באלגוריתם פיתוח בזמן לבלוקים מצומצמים (TEBD) אפשר לנו לפתוח בזמן את פונקציית הגל של מצב היסוד והמצב המעורער אותם מצאנו ובעזרתם לחשב את פונקציות הקורלציה הדינמיות ומהן את הפונקציה הספקטרלית.

כדי להבין את התהליכים המובילים ליצירת נוזל טריונים, ניתחנו את הקשר בין אינטראקציות בין חלקיקים ותנאי שיווי משקל (איכלוסים אלקטרוניים) שונים. נמצא כי ערעור המערכת, למשל באמצעות פולס לייזר קצר וחזק, ואילוח חורים למערכת מאפשרים יחד עם קשרים מספיק חזקים בין האלקטרונים והחורים יצירה של טריונים, כך שהמערכת תהיה במצב של נוזל טריונים. המודל התיאורטי שאותו חקרנו, מצביע על כך שניתן לשלוט באופן מכוון ביצירת הטריונים באמצעות כוונון פרמטרים חיצוניים, דבר הפותח אפשרויות חדשות ליישומים מעשיים בטכנולוגיות מבוססות מוליכים למחצה.

במסגרת המחקר נמצא כי בפאזות מסוימות של המודל, כאשר היחס בין מסת החור למסת האלקטרון גדול דיו והאינטראקציות בין החלקיקים חזקות מספיק, מתאפשרת יצירה של טריונים והתארגנותם לנוזל קולקטיבי אם מתאפשרים להם תנאי אכלוס עם רוב חורים. מצב זה מתאפשר כאשר אנרגיית הקשר של הטריונים גדולה יותר מפער האנרגיה בין הפסים לבין אנרגיית הקשר של האקסיטון. כלומר אקסיטון עדיין נחות אנרגטית, ולכן לא יווצר, אבל היווצרות של טריון עדיפה אנרגטית למערכת. אנו מראים כיצד ניתן לבחון את הטענה באופן תיאורטי, ובאמצעות הפונקציה הספקטרלית שלה אנחנו מציעים גם דרך לאשש או להפריך את נוכחותם של טריונים באופן ניסויי.

מצב קוונטי של טריון או אקסיטון מתאפיין בספקטרום אנרגטי אופייני של מצבים קשורים, בעל פער אנרגיה סופי לספקטרום רציף של מצבים בלתי קשורים. ניתוח ספקטרלי באמצעות חישובי פונקציית הספקטרום הראה כי בפאזה של נוזל טריונים ובפאזה של מוליך למחצה שקרוב למבודד אקסיטונים, קיימת עדות ברורה לקיומם של מצבים קשורים ולמצבים רב גופיים בעלי שזירות קוונטית גבוה. מצבים אלה נבדלים בין מצבים אלקטרוניים פשוטים יותר, כמו מצבי בלוך עבור אלקטרונים ללא אינטראקציות, אשר גם עולים באופן טבעי מחישוב הפונקציה הספקטרלית. הסימנים הספקטרליים האופייניים של המצבים הקשורים יכולים לשמש חותמת ניסיונית לזיהוי שלהם במדידות ספקטרוסקופיות המבוססות על איטראקציות אלקטרון פוטון, כמו למשל ניסוי ספקטרוסקופיית מיפוי זוויות של פליטת אור (ARPES) ווריאציות שלו. מתודות מדידה כזאת, אשר מתבססת על התגובה לשדה אלקטרו מגנטי, מאפשרות מעקב ומדידה של מצבים אלקטרוניים, קשורים או בלתי קשורים, במערכת בשיווי משקל ומחוץ לשיווי משקל.

היבט נוסף שנחקר בעבודה זו הוא יציבות הטריונים בזמן. בדקנו כיצד הפרעות חיצוניות משפיעות על קיומם של הטריונים ועל יכולתם להיוותר כמצבים קווזי יציבים. נמצא כי בטמפרטורת האפס

תקציר

תופעות קולקטיביות במערכות קוונטיות רבות-גופים מהוות תחום מחקר מרכזי בפיסיקה של חומר מעובה. אחד מהנושאים המרתקים בתחום זה הוא היווצרות של פאזה מבודדת אקסיטונית, בה קורים אפקטים קוונטיים מסדר גבוה בשל אינטראקציות בין אלקטרונים וחורים. בפרט, התנהגותם של אקסיטונים, זוגות קשורים של אלקטרון וחור, ותפקידם ביצירת פאזות חדשות נחשבת לשאלה פתוחה ובעלת חשיבות רבה להבנת תכונות החומר במצבים מבודדים למחצה. בעבודה זו אנו עוסקים בגבול הפאזות בין פאזה מבודדת אקסיטונית לבין פאזה של מוליך למחצה (מבודד פסים עם פער אנרגיה קטן) ובוחנים את התנאים להיווצרות נוזל טריונים, מצב שבו שלשות של אלקטרונים וחורים נקשרות יחדיו לכדי קווזי חלקיקים יציבים.

המוטיבציה המרכזית למחקר זה נובעת ממספר התפתחויות ניסיוניות ותיאורטיות. התפתחות במדידת של ההתפלגות הספקטרלית (לפי תנע סריגי ותדירות) של חומרים בעלי פאזה של מבודד אקסיטונים, בעלי מעבר פאזה למוליך למחצה סטנדרטי וניסויי הולכה שהראו כי בפאזות מסוימות ניתן ליצור ולמדוד טריונים. טריונים שונים מהותית מאקסיטונים בכך שהם נושאים מטען חשמלי, ולכן מאפשרים הולכה חשמלית, בניגוד לאקסיטונים, שהם קווזי חלקיקים חסרי מטען. מאחר שטריונים הם בעלי מטען חשמלי, התרומה שלהם לתהליכי הולכה חשמלית מספקת תובנות חדשות לגבי הולכה קוונטית, דינמיקה של קווזי חלקיקים ושבירת סימטריות בחומרים מבודדים למחצה. הבנה מעמיקה של מנגנון היווצרות פאזה זו חיונית כדי לפתח טכנולוגיות חדשות המבוססות על אינטראקציות אלקטרוניות מתוחכמות וללמוד על טבעם של מצבים אלקטרוניים קשורים.

בעבודה זו אנו חוקרים את היווצרות נוזל הטריונים באמצעות מודל מערכת חד ממדית המתוארת על ידי וריאציה של המודל המורחב של פליקוב קימבל (EFKM) אשר כולל אינטראקציות בין אלקטרונים לחורים, כמו גם תלות בפער האנרגיה וביחס המסות בין החלקיקים. המודל הסריגי שבחרנו למודל, מבנה של שרשרת זיגזג כפולה במימד אחד, שואב השראה ממבנה של חומר אשר נחקר היום והוא מועמד טוב להיות מבודד אקסיטונים. לצורך הפשטות, התעלמנו מדרגת החופש של ספין האלקטרון. יצירה של סדר ארוך טווח, למשל עבור עיבוי של אקסיטונים ליצרת מבודד אקסיטונים, לא אפשרית במודלים במימד אחד על פי משפט מרמין-וגנר עבור אינטראקציות קצרות טווח. אף על פי כן, אם נניח צימוד חלש של אוסף שרשראות חד מימדיות המצומדות באופן חלש, נוכל לקבל מצבים קוונטים בעלי סדר ארוך טווח.

מערכות עם אינטראקציות מובילות למצבים עם קורלציות גבוהות והן בעיות קשות לפתרון, אנליטי או נומרי. שימוש במודל שדה ממוצע ייתן במקרים רבים הבנה חלקית למדי של הטבע הרב גופי של הבעיה. שימוש בכלים נומריים חזקים ויעילים מאפשרים לנו להרחיב את גבולות המחקר וללמוד על טבען המורכב של מערכות מרובות גופים. יתרה מכך, הוא מאפשר ליצור סימולציה במעבדה

המחקר בוצע בהנחייתה של פרופסור אנה קסלמן ופרופסור דניאל פודולסקי, בפקולטה לפיסיקה.

הכרת תודה מסורה לטכניון על מימון מחקר זה.

מעבר פאזה קוונטי במודל הייזנברג $SU(4)$ על סריג משולש

חיבור על מחקר

לשם מילוי חלקי של הדרישות לקבלת התואר
מגיסטר למדעים בפיסיקה

שי נדל

הוגש לסנט הטכניון — מכון טכנולוגי לישראל
חיפה
ספטמבר 2025
תשרי תשפ"ה

מעבר פאזה קוונטי במודל הייזנברג $SU(4)$ על סריג משולש

שי נדל